EVALUATION AND IMPLEMENTATION OF AN AU' MATED BLOOD SAMPLiNG SYSTEM FOR POSITRON EMISSION TOMOGRAPHIC STUDIES

by

Manouchehr S. Vaface

Medical Physics Unit

McGill University, Montreal

March, 1993

A Thesis submitted to the

Faculty of Graduate Studies and Research

in partial fulfillment

of the requirements for the degree of

Master of Science

in Medical Physics

EVALUATION OF AN AUTOMATED BLOOD SAMPLING SYSTEM FOR PET STUDIES

by

Manouchehr S. Vafaee

Medical Physics Unit

McGill University, Montreal

March, 1993

A Thesis submitted to the

Faculty of Graduate Studies and Research

in partial fulfillment

of the requirements for the degree of

Master of Science

in Medical Physics

ABSTRACT

Quantification of physiological functions with positron emission tomography requires knowledge of the arterial radioactivity concentration. Automated blood sampling systems increase the accuracy of this measurement, particularly for short-lived tracers such as oxygen-15, by reducing the sampling interval to a fraction of a second. They, however, require correction for tracer delay between the arterial puncture site and the external radiation detector (external delay), and for the tracer bolus distortion in the sampling catheter (external dispersion).

We have evaluated and implemented the "Scandinavix" automated blood sampling system and measured its external delay and dispersion. PET studies of cerebral blood flow and oxygen metabolism using simultaneous manual and automated blood sampling were analyzed and compared. We show that the results obtained with automated blood sampling are more reliable than those based on manual sampling. We also present suggestions to further improve the reliability of quantitative PET studies based on automated blood sampling.

RÉSUMÉ

La quantification de fonctions physiologiques à l'aide de la tomographie par émission de positons nécessite la concentration radioisotopique artérielle. Des systèmes d'échantillonnage automatique sont particulièrement utiles pour des marqueurs de courte demi-vie tel l'oxygène 15. Ils permettent de réduire l'intervalle d'échantillonnage à moins d'une seconde. Cependant, ces systèmes demandent des corrections pour le délai du marqueur entre le site de la ponction artérielle et le détecteur de radiation (délai externe) ainsi que pour la distorsion du bolus dans le cathéter d'échantillonnage (distorsion externe).

Nous avons mesuré le délai et la distorsion externe du système d'échantillonnage automatique "Scandtronix". Nous avons comparé des études de débit sanguin et de métabolisme d'oxygène cérébraux utilisant simultanément l'échantillonnage manuel et l'échantillonnage automatique. Nous démontrons que les résultats basés sur l'échantillonnage automatique sont plus fiables. Enfin, nous suggérons certaines améliorations pouvant augmenter encore la fiabilité des mesures quantitatives de tomographie par émission de positons à l'aide de l'échantillonnage automatique.

ACKNOWLEDGEMENTS

I sincerely thank Dr. E. Meyer, my supervisor, for his boundless contribution to the experiments and writing throughout the course of this work. This study would not have been possible without his encouragement, constructive criticism and scientific expertise. I truly appriciate his vast wealth of understanding and patience.

I wish to thank Dr. Albert Gjedde for creating such a congenial and effective environment at the PET unit, which motivates scientists to carry out high level research Having the opportunity to work with him not only gave me the chance to learn science from him but also the human aspect of science, without which, science is not meaningful.

I extend my special gratitude to Dr. Montague Cohen, for believing in me from the beginning, this gave me the momentum to carry out my course work successfully. I highly appreciate his assistance on numerous occasions.

I would also like to thank Dr. Hiroto Kuwabara for devoting his time to answering my questions which were sometimes tedious, but helped to improve my data.

I am grateful to my friends Drs. Hitoshi Fujita and Leonardo Ribeiro for patiently helping me in different aspects of this project and teaching me whenever I needed it.

I also thank the technical staff of the McConnel Brain Imaging Centre for their assistance.

This work was supported by Medical Research Council (Canada) grant SP-30 and the Quebec Heart Foundation.

TABLE OF CONTENTS

CHAPTER 1

INTRODUCTION

1.1 Outline and Scope of Thesis

The work carried out for the preparation of this thesis, including literature review, experimentation, presentation and application of the results, is summarized here following the structure outlined below.

Chapter 1 describes the basis of PET with some of its major applications, emphasising the importance of accurate blood data (arterial input function) which is best acquired with an automated blood sampling system (ABSS).

In chapter 2, we focus on PET studies that use oxygen-15 as a tracer. In particular, we discuss the measurement of cerebral blood flow as well as oxygen metabolic rate by means of PET. The underlying models are described and the corrections to be applied to the automatically sampled arterial input function (radioactive decay, calibration, external delay and dispersion) are explained.

Chapter 3 describes the Scanditronix automated blood sampling system which was used in this thesis. We demonstrate the importance of automated blood sampling in PET studies with short-lived tracers. The components of the ABSS such as the detector and the pump together with its associated catheter system are characterized in terms of reproducibility and linearity. The experiments for the determination of the external delay and dispersion and their

verification by means of simulation studies are explained.

In chapter 4, we show that, after careful application of all of the required corrections, the automated blood curve closely resembles the manual one which is used as a reference.

Chapter 5 is devoted to the analysis of CBF and CMR_{O_2} data obtained with both manual and automated blood sampling. The results are compared and the reliability of the data obtained with the ABSS is examined.

Finally, in chapter 6 we critically discuss the problems related to automated blood sampling based on our results and experience. We also touch upon the question of the validity of using uniformly labeled aqueous solutions rather than the individual tracers used in the PET studies themselves for the evaluation of automated blood sampling systems. Investigation of this interesting problem will require further work which, however, is beyond the scope of this thesis.

1.2 The Physical Basis of PET

Unstable proton-rich nuclei decay by two processes: (a) by electron capture (EC), where the nucleus captures an orbital electron, or (b) by β^+ decay, where a proton is transformed into a neutron under emission of a positron and a neutrino. The positron is the antiparticle of the electron. After travelling a short distance, the positron will combine with an electron and undergo annihila-

tion. Upon annihilation, the masses of the electron and the positron (equivalent to 2×511 keV) are converted to electromagnetic radiation. In order to conserve both energy and linear momentum, the electromagnetic radiation appears in the form of two 511 keV gamma rays which are emitted under an angle of approximately 180° to each other (since the electron and the positron in general are never entirely at rest at the time of annihilation, there is always a net momentum with the result that the two annihilation photons are emitted at about 179.5° to each other). It is this annihilation radiation that can be detected externally. It is used to measure both the location and the quantity of a positron emitter in a medium.

The external detection and localization of a positron emitter inside an object take advantage not only of the fact that the two annihilation photons are emitted at 180° to each other, but also of the fact that they are created simultaneously. Simultaneous or coincident detection of these two photons by detectors positioned on opposite sides of an object places the site of annihilation on or about a line connecting the centers of the two detectors. If the annihilation originates outside the volume between the two detectors, only one of the photons can be detected, and since the detection of a single photon does not satisfy the coincidence condition, the event is rejected [1]. Figure 1.1 illustrates

the annihilation coincidence detection process.

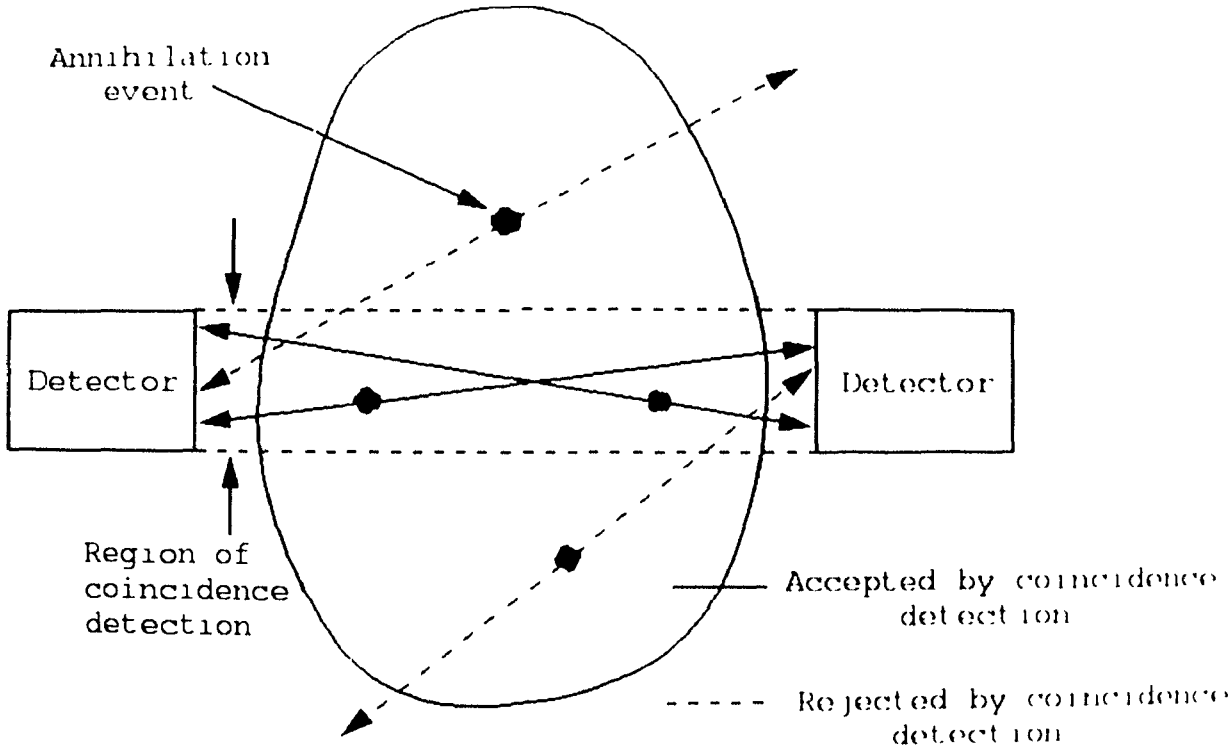

Figure 1.1 Principle of annihilation coincidence detection.

1.3 Early PET Studies

The use of positron emitting radioisotopes was first proposed in 1951 for the localization of brain tumors by Wrenn et al. [2]. Shortly after that, Sweet and Brownell [3] described the first practical non-tomographic positron imaging device in 1953. In 1966, Yamamoto and Robertson [4] published the first physiological application of positron emission tomography. They used positron emitting ^{79}Kr for the measurement of cerebral blood flow. It became rapidly apparent that PET could be used for the noninvasive in-vivo determination of human biological function, normal or pathological, due to its ability to provide quantitative information not only of the tissue radioactivity of a given radiopharmaceutical (μCi·ml^{-1}) but also, through the use of appropriate physiological models, of quantities such as cerebral blood volume (CBV), cerebral blood flow (CBF) as well as cerebral oxygen and glucose metabolic rates (CMR_{O_2}; CMR_{glc}) [5,6,7].

In practice, PET images visualizing these quantities may be reconstructed from contiguous slices to show transverse, coronal or sagittal views.

1.4 Major Applications of PET

The study of CBF, CBV, CMR_{O_2} and CMR_{glc} represents a major area of cerebral PET research. Models have also been developed for the measurement

ment of regional pH [8,9] as well as for the study of blood brain barrier function [7] and protein synthesis [10]. An important, more recent field of PET research concerns the investigation of a number of neuroreceptors and transmitters which has gained increased interest in the recent past [11]. One research application of PET, assisted by magnetic resonance imaging (MRI), which has become particular fashionable over the past few years is the investigation of cognitive function by means of CBF activation studies [12]. In such studies correlation of function and anatomy is achieved by the 3-dimensional correlation of PET (function) and MRI (anatomy) information.

Although the research potential of PET has always been recognized, an increasing number of clinically useful applications have been identified more recently. These include 1) identification of viable but compromised myocardium in patients with advanced ischemic heart disease [13] considered for by-pass surgery, 2) distinction between recurring tumor tissue and radiation necrosis [14], 3) identification of seizure foci in epileptic patients [15]. Other clinical applications might arise from the study of patients with transient ischemic attacks [16] and acute stroke [17-18] using measurements of local cerebral blood flow, blood volume as well as oxygen and glucose metabolic rates. The study of neuroreceptor transmitter function in movement disorders [19] (e.g. Huntington's and Parkinson's disease) as well as in mental disorders [20,21,22] (e.g.

schizophrenia and Alzheimer's disease) also holds some definite clinical promise. Finally, the presurgical evaluation of patients suffering from a number of cerebral lesions (arteriovenous malformations, tumors, epilepsy) located in so-called eloquent cortical areas (sensory-motor cortex, speech areas etc.) by means of functional CBF activation studies has been explored successfully [23,24]. It should be noted that a number of PET centers primarily dedicated to clinical applications are presently being established.

1.5 Dynamic PET Studies

Functional information such as rCBF may be derived from a single tomographic tissue count image together with the appropriate blood data [25,26,27,28]. A more flexible approach is to acquire a sequence of images (dynamic scan) and to calculate the desired parameter(s) by means of a least squares regression, or curve fitting, procedure which tries to match the measured tissue time-activity curve with that predicted by a given model [7]. However, count rate restrictions together with the limited timing resolution of PET, the computationally intensive task of serial image reconstruction and pixel-by-pixel curve fitting make the generation of functional images by this approach a tedious task. It has nevertheless been used to estimate CBF for extended brain regions of interest [29-31].

The generation of quantitative functional images such as CBF, CBV and

CMR_{O_2} maps requires the knowledge of the arterial tracer concentration as a function of time. In the past, this information has been obtained from manual sampling of arterial blood at intervals as short as 5 s [26]. However, manual determination of the arterial input function requires accurate timing of sample withdrawal and counting times which makes it error prone and imposes a practical limit to the sampling rate. This method further demands numerous personnel and imposes an additional radiation risk to workers. Therefore, automated blood sampling systems have been recently developed to overcome these problems.

1.6 Automated Blood Sampling Systems

The principle underlying present automated blood sampling systems consists in withdrawing, by means of a pump, arterial blood through a catheter which passes in front of a radiation detector. A number of variants of such systems exist. Hutchins et al. [32] have developed an automatic blood sampling system that uses a peristaltic pump along with a plastic scintillation detector which is sensitive to energetic positrons. Kanno et al. [33] have used a scintillation detector together with a Harvard withdrawal pump. Eriksson et al. [34] have compared the use of a single plastic scintillator which detects positrons with the use of a coincidence BGO detector pair which detects the annihilation

photons. Their system also uses a peristaltic pump. Nelson et al. [35] use a single NaI(Tl) detector to detect one of the two 511 keV annihilation photons along with a withdrawal pump.

In order to obtain reliable results, the background sensitivity of these systems should be minimized. In this regard, the coincidence system of Eriksson et al. [34] appears to be particularly well designed in that its gamma background count rate is practically negligible. The systems proposed by Kanno et al. [33] and Nelson et al. [35] have the advantage of using a withdrawal pump since, based on our experience, the adjustment and maintenance of a constant withdrawal flow rate is more difficult to achieve with a peristaltic pump.

Automated blood sampling is superior to manual sampling in several ways. First, it demands minimum manual intervention and thus reduces the radiation hazard to personnel. Second, the sampling interval can be reduced to a fraction of a second. However, corrections for external tracer delay (i.e. the time difference between the arterial site where blood is withdrawn and the detector where the count rate is measured) and external dispersion (i.e. the difference in the degree of distortion in the blood curve resulting from the dispersion of the tracer bolus in the additional length of catheter from the peripheral sampling site to the detector) must be carefully applied to the blood data acquired with such blood sampling systems [34] before it can be used.

CHAPTER 2

OXYGEN-15 STUDIES WITH PET

2.1 Introduction

Among the positron emitting radioisotopes frequently used in PET, oxygen 15 (^{15}O) is the one with the shortest physical half-life ($T_{1/2}$=2.035 min) and the most energetic positron ($E_{max_{\beta+}}$=1.72 MeV). Both these facts have their consequences for the use of ^{15}O in PET imaging. The short physical half-life makes the on-site production of ^{15}O by a medical cyclotron mandatory. On the other hand, it allows multiple ^{15}O studies to be performed on the same subject within a short time with limited radiation exposure and negligible interference from residual radioactivity. This possibility has given rise to some exciting applications of ^{15}O such as metabolic mapping of functional activity of the brain by means of blood flow activation studies [12]. The large positron energy of ^{15}O results in a resolution broadening effect of $\geq$ 1 mm (FWHM) [1]. The major applications of ^{15}O in PET imaging, at present, are centered on the study of brain function [36]. The compounds used include $C^{15}O$ for the measurement of cerebral blood volume (CBV), $CO^{15}O$ and $H_2{}^{15}O$ for the measurement of cerebral blood flow (CBF), and $O^{15}O$ which, together with the former studies, allows to estimate the cerebral oxygen extraction fraction (E_{O_2}) and oxygen utilization rate (CMR_{O_2}). Furthermore, the oxygen consumption of the brain has recently

been measured directly from a single inhalation of $O^{15}O$ using the time-weighted integration method [5].

2.2 Cerebral Blood Flow (CBF)

The measurement of regional CBF is one of the most frequently performed PET procedures. Often, PET CBF investigations are carried out as independent studies in their own right such as for instance in physiological blood flow activation studies [12].

2.2.1 Theory

Most present PET CBF methods use $H_2{}^{15}O$ and are based on the Kety-Schmidt one-compartment model for diffusible inert tracers [37,38]. However, since water is not a freely diffusible tracer [26,39], i.e. its capillary first-pass extraction fraction, E_o, is smaller than one, an additional compartment is necessary to account for the non-extracted residual intravascular radioactivity. In the following paragraphs, the one- and two-compartment models are briefly described.

2.2.1.1 One-compartment Model

The one-compartment model assumes that water is perfectly diffusible, i.e. the transfer of tracer from blood to brain tissue is only limited by blood

flow (Fig. 2.1A). In this model, a volume of tissue, V_t, is perfused with tracer which enters the compartment through the arterial blood stream at a flow F [ml·min^{-1}] and concentration C_a [Bq·ml^{-1}]. The compartment loses the tracer on the one hand through venous outflow with concentration C_v and, on the other hand, via radioactive decay (λ is the decay constant which, in the case of ^{15}O, is 0.34 min^{-1}). The rate of change in the amount of $H_2{}^{15}O$ in tissue, Q, can then be expressed as:

$$\frac{dQ}{dt} = F(C_a - C_v) - \lambda Q \qquad (2.1)$$

Equation (2.1) is based on the Fick principle which expresses the law of conservation of mass, adapted here to include the physical decay of tracer [37] We define the tissue tracer concentration C=Q/W_t [Bq·g^{-1}] and the venous, or compartmental, tracer concentration C_v=Q/V_d [Bq·ml^{-1}], where W_t is the weight of the tissue element [g] and V_d the tracer distribution volume [ml]. We further define the equilibrium tissue-blood partition coefficient of the tracer, p=C/C_v = V_d/W_t [ml·g^{-1}], the tissue blood flow f=F/W_t [ml·min^{-1}·g^{-1}] and assume that C_a and C have been corrected for radioactivie decay. Then, equation (2.1) becomes:

$$\frac{dC}{dt} = fC_a - (\frac{f}{p})C \qquad (2.2)$$

With C and C_a being variable with time, integration of equation (2.2)

with the initial condition C(0) = 0 yields:

$$C(t) = f \cdot \int_0^t C_a(\tau) e^{-\frac{f}{p}(t-\tau)} d\tau \tag{2.3}$$

Since PET, in general, does not measure the instantaneous tissue concentration, C(t), but rather its integral over a given time (frame length T_1 to T_2), the following operational equation is used to determine the blood flow, f:

$$C(t) = \int_{T_1}^{T_2} C(t) dt = \int_{T_1}^{T_2} f e^{-k_2 t} \int_0^t C_a(\tau) e^{k_2 \tau} d\tau dt \tag{2.4}$$

where C(t) is the total number of radioactive events per unit weight of brain tissue detected by the tomograph during the scan, C_a the arterial concentration and k_2=f/p.

2.2.1.2 Two-compartment Model

Since for $H_2{}^{15}O$ there is a diffusion barrier between the vascular compartment and the brain tissue, two compartments are necessary for the description of its dynamics [40] (Fig. 1.2B). We define the unidirectional clearance of a substance (e.g. $H_2{}^{15}O$) from blood by brain tissue, K_1, and its first-pass extraction fraction, E_o, with F being the blood flow. These three quantities are related as follows: $K_1 = E_o F$. If we further define k_2 as the fractional clearance (or rate constant), describing the washout of exchangeable tracer from the extravascular space and Q_e as the quantity of exchangeable labeled material in the

extravascular portion of the tissue, then Fick's equation can be written as:

$$\frac{dQ_e}{dt} = K_1 C_a - k_2 Q_e \tag{2.5}$$

Introducing the initial vascular volume of distribution for water in brain, V_o, so that

$$Q = Q_e + V_o C_a \tag{2.6}$$

we arrive at the following solution for the total observable brain radioactivity, Q:

$$Q(T) = (K_1 + k_2 V_o) \int_0^T C_a(t)dt + V_o C_a(T) - k_2 \int_0^T Q(t)dt \tag{2.7}$$

From equation (2.7), K_1, k_2 and V_o can be estimated by non linear regression or by the weighted integration method [41]. CBF may then be calculated from the relation $K_1 = E_o \cdot CBF$ if E_o is known.

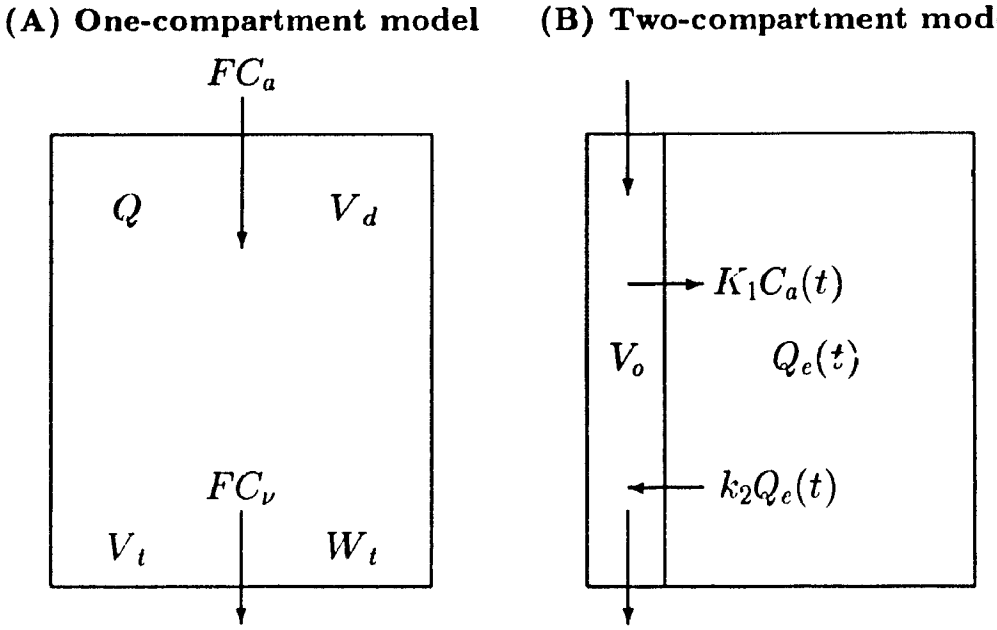

Figure 2.1 (A) One-compartment model for a freely diffusible inert tracer. Shown is a tissue element with volume V_t, weight W_t, tracer content Q, and tracer distribution volume V_d. The tissue element is homogeneously perfused with blood flow F at arterial and venous tracer concentrations C_a and C_v. (B) Two-compartment model representing intravascular (blood) and extravascular (tissue) spaces separated by the blood-brain barrier for a diffusion-limited tracer with a first pass capillary extraction fraction of $E_o<1$. K_1 is the undirectional clearance of tracer from blood into tissue and k_2 is the rate constant which describes the washout of exchangeable tracer from tissue.

2.2.2 The Arterial Input Function

As apparent from the previous paragraphs, the determination of CBF by PET requires the measurement of the arterial ^{15}O tracer concentration, called arterial input function, in addition to the quantification of the radioactivity distribution in the brain. The former information may be obtained by means of an automatic blood sampling system. As mentioned in chapter 1, this requires appropriate corrections for tracer delay and dispersion which will be discussed in the following paragraphs.

2.2.2.1 Delay Correction

The difference between the tracer arrival time in the brain and the peripheral sampling site is called internal delay. The critical dependence of the calculated CBF value on appropriate correction for this delay has been demonstrated [42,43].

One delay correction method that has been used traditionally, the so-called slope method, determines the tracer arrival time difference by linear backward extrapolation of the upslopes of the arterial and the whole brain slice radioactivity curves [33,42]. The arterial curve is then shifted along the time axis by the determined arrival time difference. Another method, the so-called global fitting method of Iida et al. [43], determines this delay by means of a least squares fitting procedure. The regional tissue curves are approximated by the time activity

curves, X(t), of the corresponding cross-sectional brain tissue slices. Based on equation (2.3), X(t) may be described as:

$$X(t) = A \cdot \int_0^t C_a(\tau + \Delta\tau) \cdot e^{-B(t-\tau)} d\tau \tag{2.8}$$

where $\Delta\tau$ is the global delay between the measured arterial and the whole brain slice curve. A and B are arbitrary parameters which, together with $\Delta\tau$, can be determined by means of non-linear least-squares fitting. Typical values for $\Delta\tau$ lie between 4 and 8 s [43]. In the present work, we have adopted this method to evaluate the external delay of the ABSS.

2.2.2.2 Dispersion Correction

The correction for the difference in the degree of distortion in the curve shape of the arterial input function resulting from the dispersion of the tracer bolus in the blood vessels between the heart and the brain on the one hand and between the heart and the radial artery (sampling site) on the other hand, is called internal dispersion correction. Appropriate dispersion correction of the arterial input function is essential for the quantification of CBF [44].

Let $C_a(t)$ be the true and g(t) the peripherally measured, dispersed input function. These quantities are related to each other by the dispersion function, d(t), as follows:

$$g(t) = C_a(t) * d(t) \tag{2.9}$$

where the asterisk stands for the convolution operation.

The dispersion function, d(t), for the monoexponential model proposed by Iida et al. [44], is:

$$d(t) = \frac{1}{\tau} exp(\frac{-t}{\tau}) \tag{2.10}$$

where τ is the dispersion time constant. Using Laplace transforms [33], $C_a(t)$ can then be expressed as:

$$C_a(t) = L^{-1}[\frac{G(s)}{D(s)}] = L^{-1}[\frac{s + 1/\tau}{1/\tau} G(s)] \tag{2.11}$$

where D(s) and G(s) are the Laplace transforms of d(t) and g(t), respectively, and L^{-1} means the inverse Laplace transform operation.

Using Laplace transform tables, equation (2.11) is solved to yield [42]:

$$C_a(t) = g(t) + \tau(\frac{dg}{dt}) \tag{2.12}$$

In practice, the dispersion time constant may be determined by introducing a step function of radioactivity into the blood sampling system and measuring its response function.

The distortion in the input function due to the additional length of the automatic blood sampling catheter is called external dispersion. The automatically sampled blood curve has to be corrected for this external dispersion. The external dispersion time constant may be determined, using equations (2.9) to (2.12) and by defining $C_a(t)$ as the arterial concentration determined manually,

e.g. from the radial artery, and g(t) as the concentration measured with the external radiation detector. The procedures for delay and dispersion correction used in this thesis will be discussed in detail in chapter 3.

2.3 Cerebral Metabolic Rate of Oxygen (CMR_{O_2})

The *in-vivo* determination of regional cerebral oxygen utilization, or cerebral matabolic rate of O_2 (CMR_{O_2}), was pioneered by Ter-Pogossian and associates [45,46] who used the bolus injection of ^{15}O-labeled water and ^{15}O-oxyhemoglobin together with conventional external monitoring techniques to measure CBF and the first pass extraction fraction, E_o, of oxygen, respectively. CMR_{O_2} is then calculated as the product of CBF, E_o and the arterial oxygen content, $[O_2]_a$. These results were validated by comparison with hemispheric CMR_{O_2} values obtained from direct measurements of differences in arteriovenous oxygen content and assuming E_o and the net extraction fraction at steady-state, $(C_a^{O_2}\text{-}C_v^{O_2})/C_a^{O_2}$, to be equal. Here, $C_a^{O_2}$ and $C_v^{O_2}$ are the arterial and venous oxygen concentrations at steady-state.

Current PET techniques for the measurement of CMR_{O_2}, which include the continuous inhalation or steady-state method by Frackowiak and associates [28] and the sequential bolus approach of Mintun and colleagues [47], are based on the same basic principle. With these techniques, CMR_{O_2} is calculated from a

series of three PET studies which includes the measurements of CBF, CBV and oxygen extraction fraction, OEF. Such a multitracer study may last from 30 min (bolus method) to over an hour (steady-state method). Faster methods to measure CMR_{O_2} have been proposed [48,49]. Recently, Ohta et al. [5] have shown that CMR_{O_2} can be measured after a single inhalation of ^{15}O-labeled molecular oxygen. In this case, hemoglobin is labeled by inhaling $O^{15}O$ as a bolus (60-80 mCi). For that reason, the arterial time-activity curves from CMR_{O_2} studies look somewhat different from those obtained in CBF studies, where the tracer is injected intravenously. As in the case of CBF measurements, the arterial time-activity curves in CMR_{O_2} studies also require the corrections for tracer delay and dispersion.

CHAPTER 3

AUTOMATED BLOOD SAMPLING SYSTEM (ABSS)

3.1 Introduction

Dynamic studies with positron emission tomography (PET) allow to measure the kinetics of a variety of radiopharmaceuticals in the tissue of living humans or animals.

In order to derive physiological parameters from such studies, however, the PET data of tissue uptake must be compared with model predictions. A quantitative analysis of such models requires the knowledge of the time course of the tracer concentration in arterial blood or plasma, the so-called input function or arterial blood curve [1]. The model parameters, representing the physiological quantities of interest, can then be determined by various parameter estimation techniques [1] such as non-linear least squares fitting [7] or time-weighted integration [41,50].

In heart studies, it is possible to obtain the blood curve from the PET images directly by generating a time-activity curve from a region of interest (ROI) corresponding to the blood pool of the left ventricle or by placing a positron sensitive detector into the left ventricle [44]. When imaging other organs such as the brain, the blood curve must be obtained from arterial samples which are usually withdrawn from a peripheral artery (e.g. radial artery). These samples

are assayed in a well counter, which is calibrated with respect to the tomograph.

For dynamic studies, the blood sampling task is not trivial. Manual sampling usually involves taking blood samples as fast as possible for the first few minutes after tracer injection when the blood concentration changes rapidly. As the kinetics slow down when the tracer reaches quasi-equilibrium with the tissue, longer time intervals may be used. Maintaining a rigorous sampling schedule and avoiding artefacts on the blood curve is difficult with manual sampling [34]. Automated blood sampling systems have therefore been designed [33,34,32,35].

3.2 The Scanditronix ABSS

In this thesis, we have evaluated and implemented such a system (Scanditronix) [34] for the measurement of blood tracer activity. It consists of a radiation detector unit and a peristaltic pump that continuously withdraws blood through the detector via a plastic catheter. A computer monitors the detector system and communicates the results (the blood file) to the host computer (Fig 3.1). The host computer is a Micro VAX II, manufactured by Digital Equipment Corporation (DEC). It runs under the VAX/Micro VMS operating system. The format of a sample blood file is given in Appendix I.

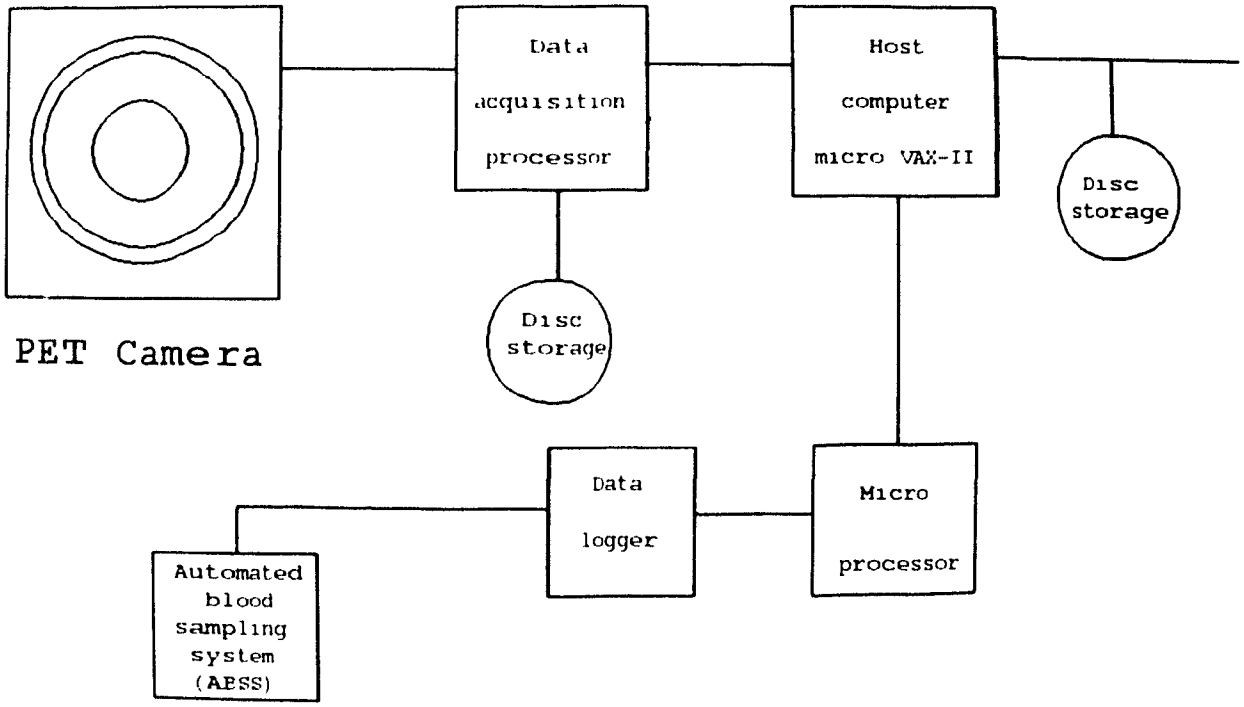

Figure 3.1 Block diagram of automated blood sampling system in relation with the positron camera.

3.2.1 Detector System

There are various ways to detect positron emitting tracers. One is to detect the positrons themselves [1,50]; the other way is to detect the two annihilation gamma quanta with a coincidence technique [1,51]. Both techniques are presently being used [32,51] in ABSSs. The positron detector requires a different calibration factor for each positron emitter which depends upon the kinetic energy of the positron. In addition, it is very sensitive to blood density differences. For coincidence detector systems, BGO (bismuth germanate) is the detector material of choice because of its excellent stopping power [51] for the 511 keV annihilation quanta.

In our system, coincidence detection is being used which has the advantage of a very low background sensitivity. The detector unit consists of four BGO crystals housed in a light proof box with outer dimensions $65\times50\times190$ mm. The crystal dimensions are $30\times25\times20$ mm. The photomultiplier tubes are of the Hamamatsu R647 type with integral magnetic and electrostatic (μ-metal) shields. The detector unit is surrounded by a 3 cm thick lead shield. The system contains a buffer board to drive 50 Ohm cables. The high voltage for the photomultiplier tubes is supplied through a current limiting resistor from the tomograph's high voltage power supply. Figures 3.2 and 3.3 show the details of the detector system.

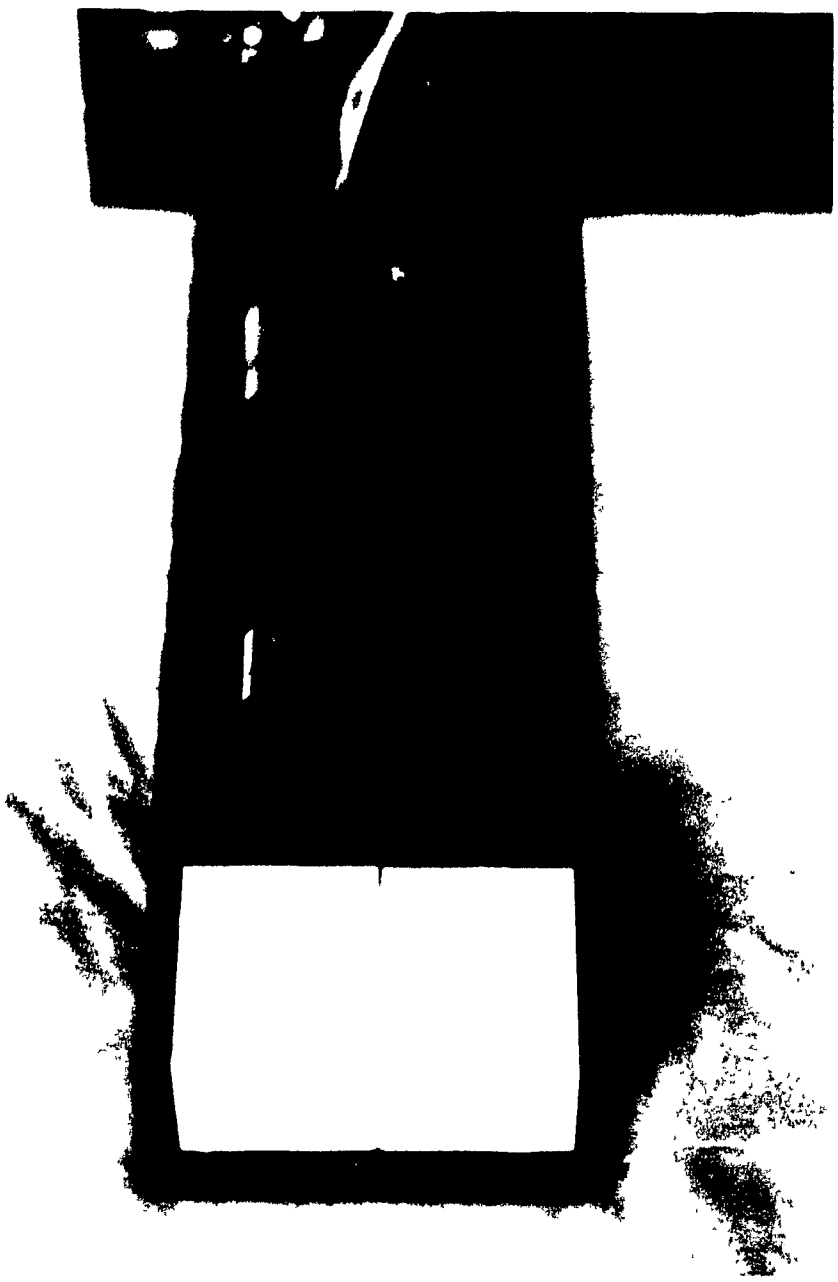

Figure 3.2 Coincidence detector pair.

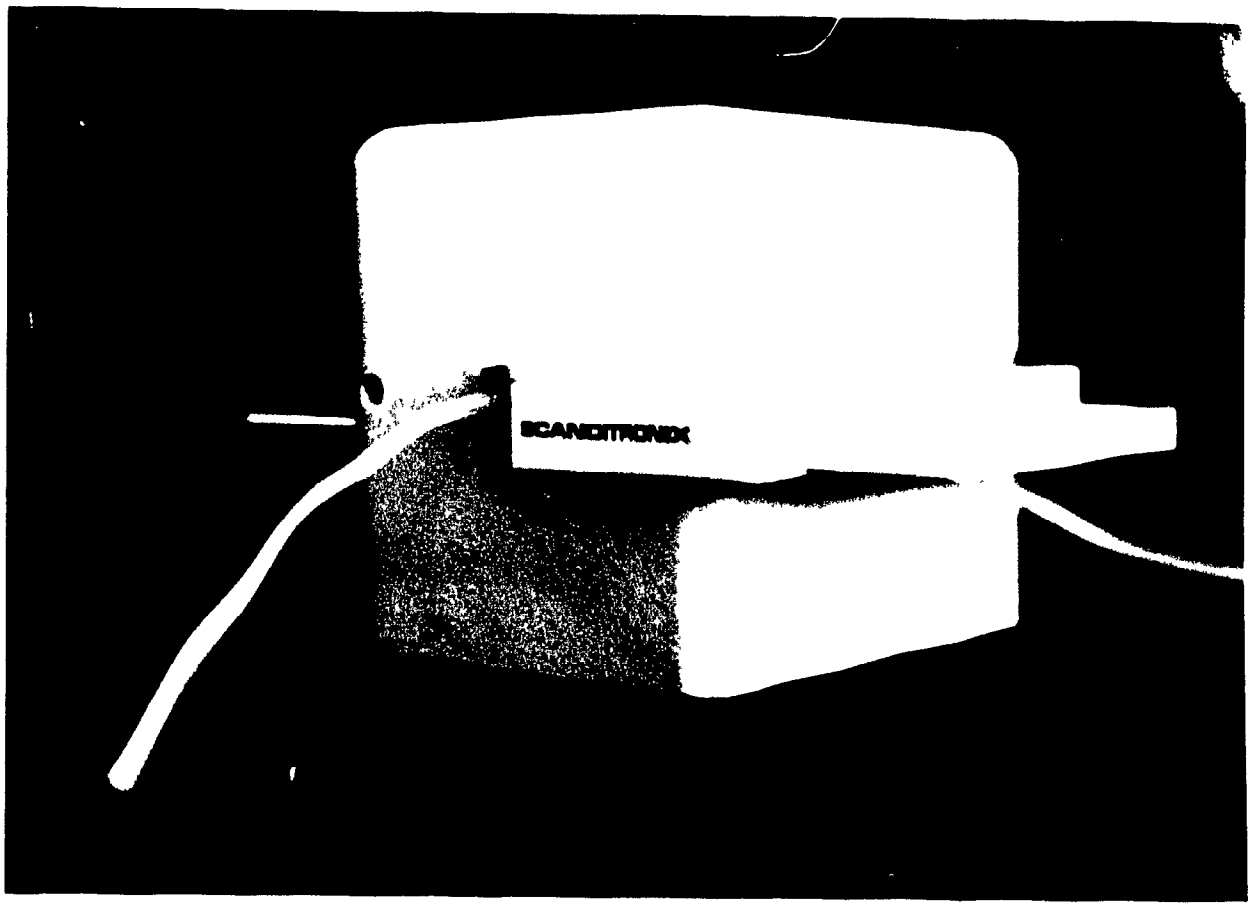

Figure 3.3 Overall view of detector system with catheter.

3.2.2 Pumping System

Withdrawal of arterial blood is achieved by a peristaltic pump (Alitea C-4, Sweden). It can circulate a maximum of 9.5 $ml \cdot min^{-1}$ of blood through the sampling catheter at a rotator speed of 49 revolutions per minute (R.P.M.). A blood withdrawal rate of 7.5 $ml \cdot min^{-1}$ corresponding to 40 R.P.M. is routinely selected which is roughly the same as during manual sampling. The pump is not under computer control; it is started and stopped manually by the operator [51]. Figure 3.4 shows the peristaltic pumping system.

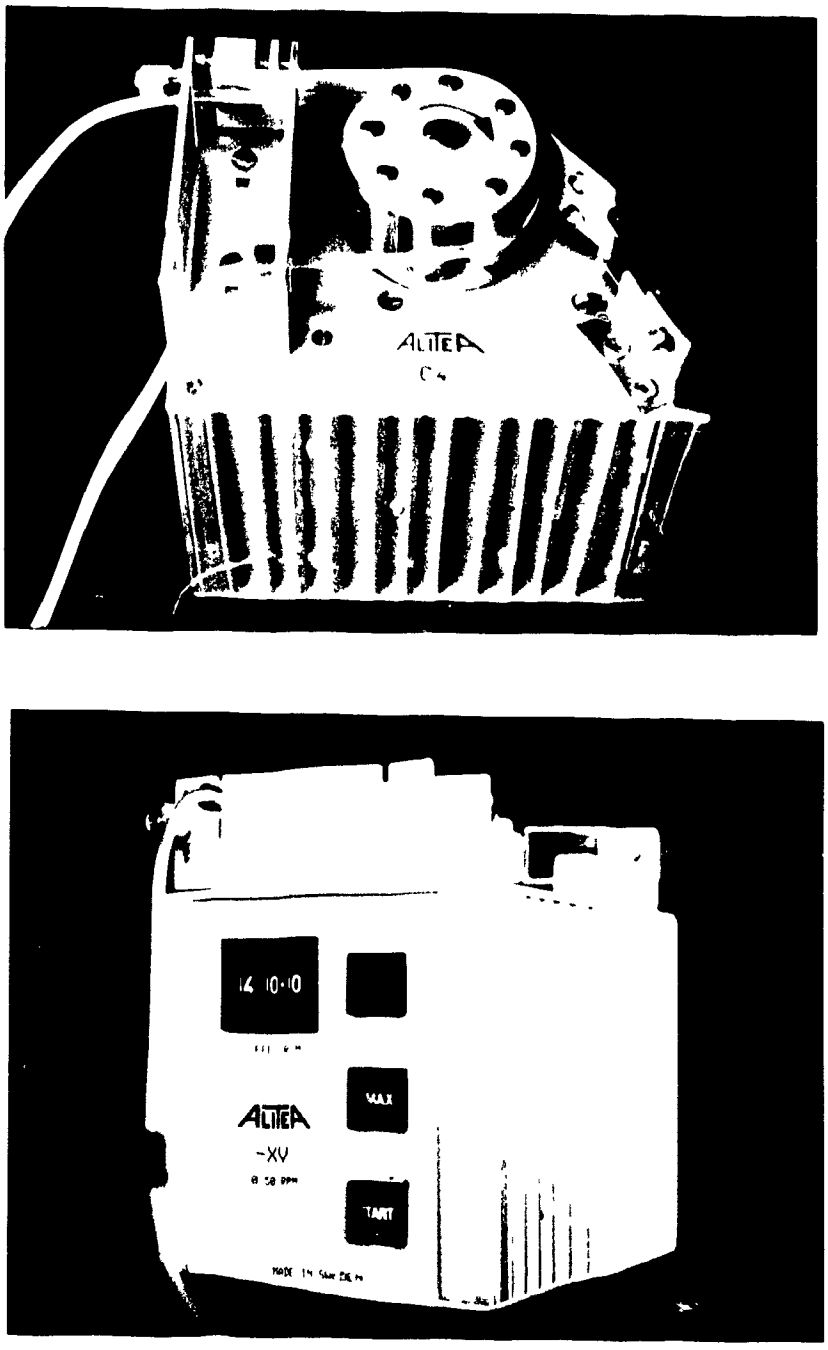

Figure 3.4 Pumping system with withdrawal catheter.

3.2.3 Catheter System

The standard catheter used for the withdrawal of blood through the detector system is 40 cm long with outer and inner diameters of 3.457 mm and 2.057 mm, respectively (Radicath, Radiplast AB, Sweden). In practice, two such catheters are connected by a small plastic tube so that there is no diameter difference at the junction. It is secured in a slit along one end of the detector unit and then placed between the rollers and the guide of the pump and tightened by means of a clamp (Fig. 3.5). The slit in the detector can accommodate catheters with a diameter up to 4 mm and the pump can rotate only clockwise at a rate of 1-49 R.P.M.

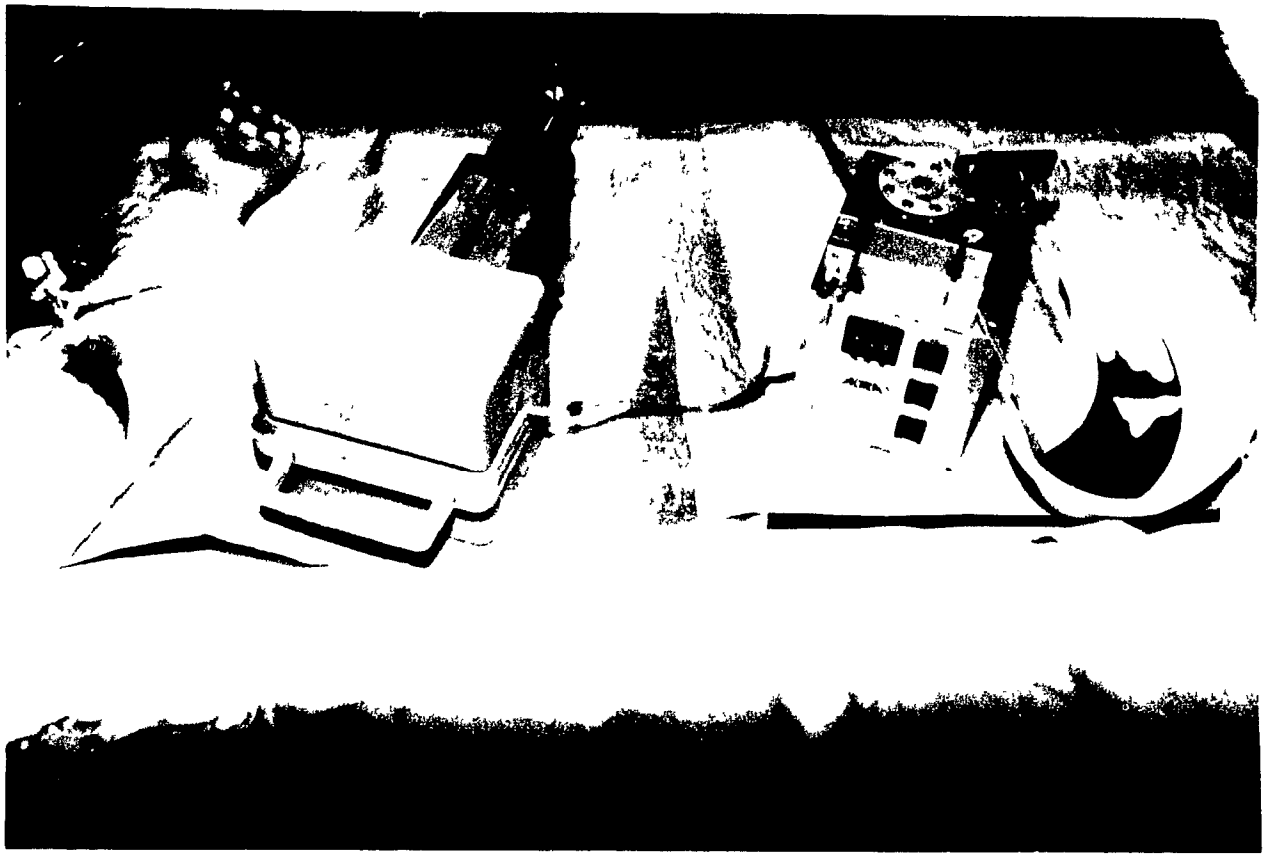

Figure 3.5 Automated blood sampling system including detector, pump and catheter.

3.3 Evaluation of the Physical Characteristics of the ABSS

In order to check the performance of the ABSS, its physical characteristics were studied and verified. This included evaluation of the reproducibility with respect to the withdrawal rate and the linearity of the system response as well as the determination of the external tracer delay and dispersion time constant.

3.3.1 Preparation of Radioactive Solution

Instead of using labeled blood during the experiments with the ABSS, we used a radioactive solution with the same average viscosity as that of blood. This was achieved by dissolving 30 grams of sugar per 100 ml of distilled water. The resulting solution had a viscosity of 2.8 centipoise at 20°C. The viscosity of human blood varies between 2-4 centipoise at 20°C [52]).

Because of the short half-life of ^{15}O ($T_{1/2}$=2.035 min), we decided to use Ga-68 EDTA (ethylenediaminetetraacetic acid) with a half-life of $T_{1/2}$=68 min which imposed less time constraints on the experimentation.

In order to prepare the Ga-68 EDTA solution, 44.58 g of $Na_2HPO_4 \cdot 7H_2O$, 11.73 g of $NaH_2PO_4 \cdot H_2O$ and 0.456 g of EDTA were dissolved in 250 ml of water to give a 5×10^{-3} mol EDTA concentration with a pH=7.0. The solution was then passed through a Ga-68 generator from which the radioactive Ga-68 EDTA solution was eluted.

3.3.2 Reproducibility Tests

The reproducibility of the system's performance with respect to changes in withdrawal rate ($ml \cdot min^{-1}$) were tested for different positions of the catheter tension adjustment screw.

3.3.2.1 Withdrawal Rate

The reliability of the pumping system was tested by varying the withdrawal rate between 3.5 and 7.5 $ml \cdot min^{-1}$ and then measuring the withdrawal volume of solution after different times. If we call V the withdrawal volume and W the withdrawal rate, the relationship between V, W and withdrawal duration t, is :

$$V = W \times t \tag{3.1}$$

The expected linear relationship between V and t for a given withdrawal rate, W, was confirmed (Figure 3.6).

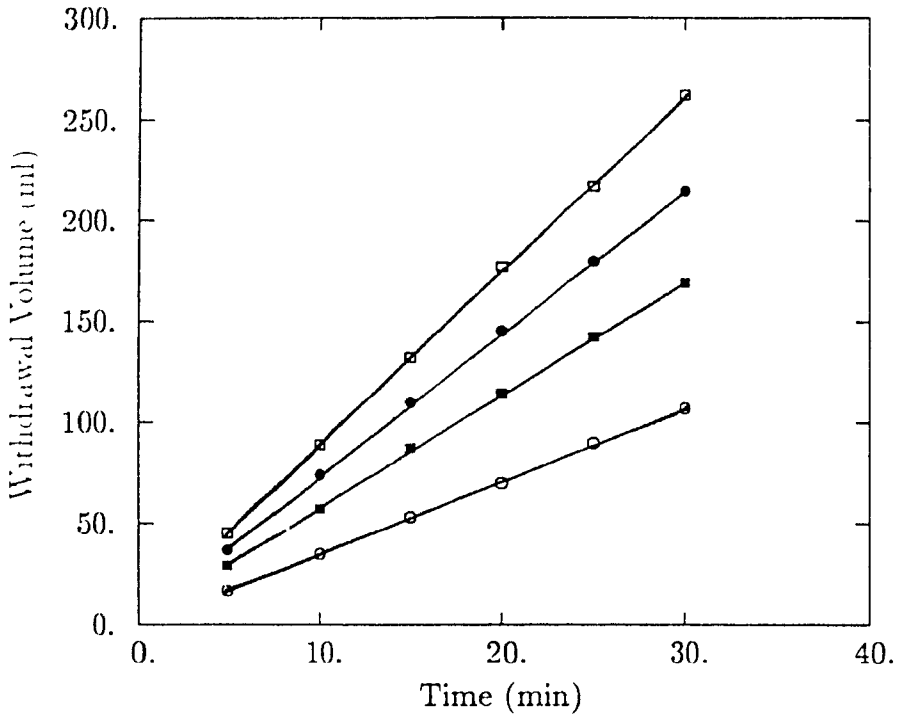

Figure 3.6 Performance of pumping system at withdrawal rates of 9.5 (□), 7.5 (●), 5.5 (■) and 3.5 (○) ml·min^{-1}.

3.3.2.2 Catheter Tension Adjustment Screw

A critical component of the ABSS is an adjustment screw on top of the pump which affects the tightness of the catheter guide, which in turn affects the catheter flow rate. In order to check the effect of the position of this adjustment screw on the catheter flow rate, and in particular the reproducibility of its adjustment, the following test was performed. The pump was set at 40 R.P.M. and the tension screw adjusted to yield a withdrawal volume of 7.5 ml in one minute. The adjustment screw was then untightened and the withdrawal catheter completely removed from the pump. A new catheter was installed and the screw adjusted to the same position as before and the withdrawal volume for one minute measured again for the same 40 R.P.M. setting. This procedure, which was intended to simulate the repeated set-up of the ABSS for individual PET studies, in all of which a withdrawal rate of 7.5 $ml \cdot min^{-1}$ was desired (standard withdrawal rate for this system), was repeated 10 times. The average withdrawal volume from these 10 experiments was: $V = 7.40 \pm 0.55$ $ml \cdot min^{-1}$. Although this result demonstrates that, with the necessary care, satisfactory reproducibility can be achieved, we believe that a peristaltic pump is not the ideal device for this application because, after prolonged use, the mechanical parts such as rollers, guide and adjustment screw might start to affect the performance of the system in an unpredictable manner. We would suggest replacing

it with a syringe withdrawal pump which appears to be more reliable and is presently being used in other ABSSs [33,35].

Table 3.1 Pump R.P.M setting vs. withdrawal rate.

R.P.M.	withdrawal rate ($ml \cdot min^{-1}$)
20	3.5
30	5.5
40	7.5
49	9.5

3.3.3 Linearity Test

One of the most important requirements for an ABSS is the linearity of its response to changes in blood radioactivity concentration.

In order to check the linearity of the ABSS, the following experiment was performed with Ga-68 EDTA. A radioactive solution with a known concentration was first prepared. The count rate was then measured with the ABSS as a function of time after the introduction of a step input of radioactivity achieved by inserting the proximal end of the catheter into the radioactive solution. Figure 3.7 shows the result of this study. The x-axis represents the radioactivity concentration of the Ga-68 EDTA solution and the y-axis shows the detector count rate. We can see that, for concentrations between 0 and 90 μCi·ml^{-1} (corresponding to a maximum detector count rate of 19000 cps), the system response is in fact linear. Although the offset of the regression line is not zero, this should not be interpreted as representing a background count since, as apparent from Appendix I (column d), the background count rate of the coincidence detector unit of our ABSS is negligible. Rather, one might speculate that this offset represents a slight non-linearity for very low count rates. The sensitivity of the system, represented by the slope of the graph, was obtained by linear least squares regression and found to be 211 (cps)/(μCi·ml^{-1}). This value is close to that reported for a similar system by Nelson et al. [35]. Typical blood

radioactivity concentrations observed following a 40-50 mCi O-15 water bolus injection (standard water bolus CBF study) usually fall well below the maximum count rate observed in this linearity test. Consequently, the coincidence detector count rate does not require any correction for dead time losses in this range.

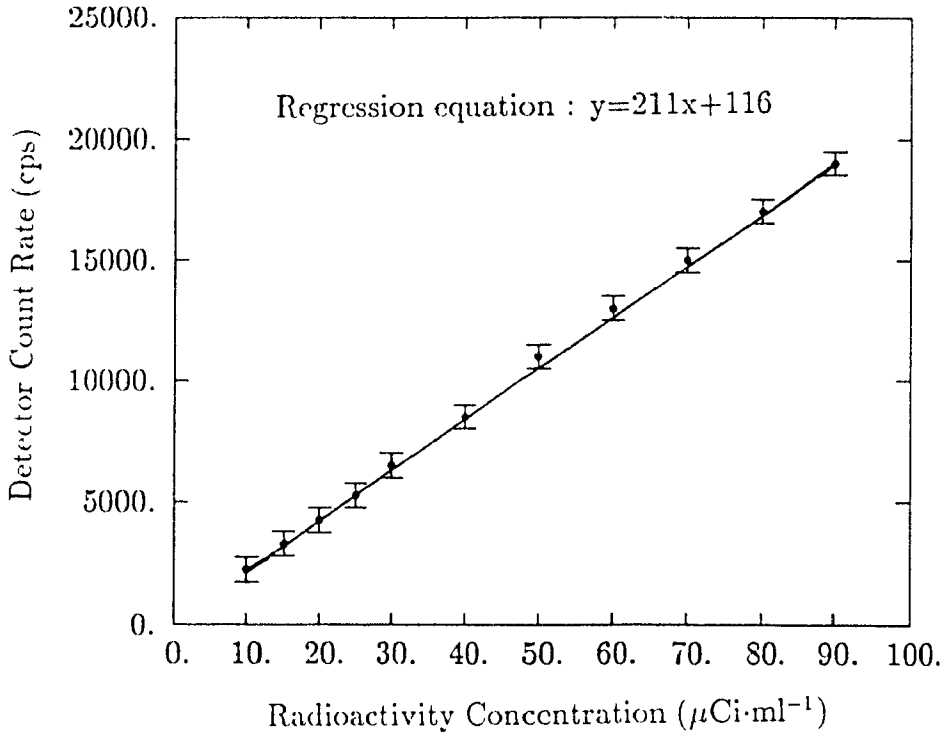

Figure 3.7 Linearity test of automated blood sampling system.

3.3.4 Simulation Studies

A number of characteristics of the ABSS were studied by means of simulation. Since the generation of sequences of random numbers obeying a given probability distribution is fundamental to such studies, a brief discussion on the generation of random number generation and poisson random variation is presented in the following paragraph.

3.3.4.1 Random Variable Generation

A random variable such as the count rate from a detector which obeys a Poisson probability distribution can be generated by means of a random number generator. The first step is to produce a sequence of independent, uniformly distributed random numbers on the interval 0 to 1 [53].

A frequently used, so-called linear congruential random number generator (R.N.G.), has the form:

$$Z(i) \equiv a \cdot \mathrm{Z(i\text{-}1)}+\mathrm{c} \pmod{m} \qquad \text{(a)}$$

$$\mathrm{i} = 1,2,3,4,5,.....\mathrm{n}$$

This R.N.G. is called mixed congruential for $c \neq 0$ and multiplicative congruential (multiplier a) otherwise. Z(0) is the initially specified (integer) number of the sequence, called seed, and each subsequent (integer) number of the sequence is obtained from its predecessor as the remainder of an integer division of the

is obtained from its predecessor as the remainder of an integer division of the right hand side of the equation (a) by the modulus m. This recursive calculation of successive numbers of the sequence is efficiently handled by computers.

From the above it is clear that no number Z(i) can exceed the value of the modulus m. The random numbers on the unit interval (0,1) are then formed as:

$U(i) = Z(i)/\ m$

Upon appropriate selection of the parameters a,c and m, it can be achieved that the random numbers Z(i) assume all values between 0 and m during one generation cycle, i.e. before Z(0) is reached again. Such a random number generator is said to have full period. This is a desirable feature for a random number generator since it assures a uniform density of random numbers over the entire interval (0,m), respectively (0,1). Furthermore, in order to obtain a reasonably high density of random numbers over the unit interval, the modulus m has to be chosen as large as possible.

The discrete random variable N, with mean value λ, obeys the Poisson distribution law if the probability for N=n is given by:

$$P(N=n) = e^{-\lambda} \cdot \lambda^{-n}/n! \qquad n=0,1,...\infty$$

Such a random variable, N, can be generated in the following manner: Let's assume we have to satisfy the condition:

$$\prod_{i=0}^{N+1} U_i < e^{-\lambda} \leq \prod_{i=0}^{N} U_i \qquad n=0,1,...$$

where $\prod_{i=0}^{N} U_i = U_0 \cdot U_1 \ldots U_N$ and the U_i's are independent, uniformly distributed random numbers on the interval (0,1) and λ is the mean value of the Poisson random variable, N, we want to generate. Then the number N, required to satisfy this condition, follows a Poisson distribution with mean value λ. It is obvious, however, that when λ is large, $e^{-\lambda}$ is small so that the number of U_i's needed to satisfy the condition may also be large and the procedure therefore time consuming. In order to achieve a time saving, use is made of the fact that, as λ increases, the distribution of random variables $Y=(N-\lambda)/\sqrt{\lambda}$ converges to a normal, or Gaussian, distribution with zero mean and variance one, denoted by G(0,1). In order to produce the Poisson random variable N, we first have to generate Y from G(0,1) and then compute, and round to an integer, the expression $N = \sqrt{\lambda} \cdot Y + \lambda$. We are now left with the generation of a normally distributed random variable, Y, which is achieved as follows: Let U_1 and U_2 again be independent uniformly distributed random numbers on the unit interval (0,1). The variables: $Y_1 = \sqrt{-2 \cdot lnU_1}\ \cos(2\pi U_2)$ and $Y_2 = \sqrt{-2 \cdot lnU_1} \cdot sin(2\pi U_2)$ are then independent. The above approximation is satisfactory for $\lambda \geq 15$ [53] For $\lambda < 15$, the exact procedure described at the beginning of this paragraph has to be used.

For the simulation studies described in the following paragraphs, a system-supplied uniform random number generator (RANO) together with a subroutine

which returns a normally distributed deviate with zero mean and unit variance (GASDEV) were used (see Appendix II).

3.3.5 External Tracer Delay

The external tracer delay was measured both physically and by simulation and leaste squares fitting as described in the next two paragraphs.

3.3.5.1 Physical Delay Calculation

The tracer travel time difference between the arterial site where blood is withdrawn and the mid-point of the coincidence detector pairs where the blood tracer concentration is measured (average of coincidence count from first and second detector pair) was determined physically, i.e. by measuring the travelling time of the radioactive solution in the catheter between the sampling site and the first detector pair on the one hand and from the sampling site to the second detector pair on the other hand. This measurement was performed for four different distances between arterial sampling site and detector position. Since there was a negligible difference in count rate onset between the first and the second detector pair, we decided to use the count rate from the first one exclusively throughout this project. Table 3.2 and Figure 3.8 show the expected increase of the delay with catheter length. In addition, Table 3.2 gives a com-

parison between the measured delays and those calculated by applying equation (3.1), using a flow rate, W, of 7.5 ml·min^{-1}, a catheter diameter of 2r = 2 057 mm and a catheter length of l = 20 cm.

$$V = W \times t = l \times \pi r^2 \tag{3.2}$$

The slight difference between the measured and calculated results can be explained by the importance of the catheter radius in the calculation of t (the delay is proportional to the square of the radius) and the fact that this diameter might not be constant over the entire length. Since the standard artery detector distance (artery to mid-point of first detector pair) for our ABSS is 20 cm, the measured delay of 4.5 s (Table 3.2) is used throughout this thesis

Table 3.2 External delay for different artery-detector distances.

Artery-detector distance (cm)	Measured delay (s)	Calculated delay (s)
20	4.5 ± 0.50	4.98
35	8.5 ± 0.55	8.71
50	12.5 ± 0.87	12.4
63	15.5 ± 1.15	15.69

Values are means ± SD for n=15 experiments

Flow rate was 40 0 R P M (7 5 ml min^{-1}) and viscosity of the solution

was the same as that of blood (2-4 centipoise)

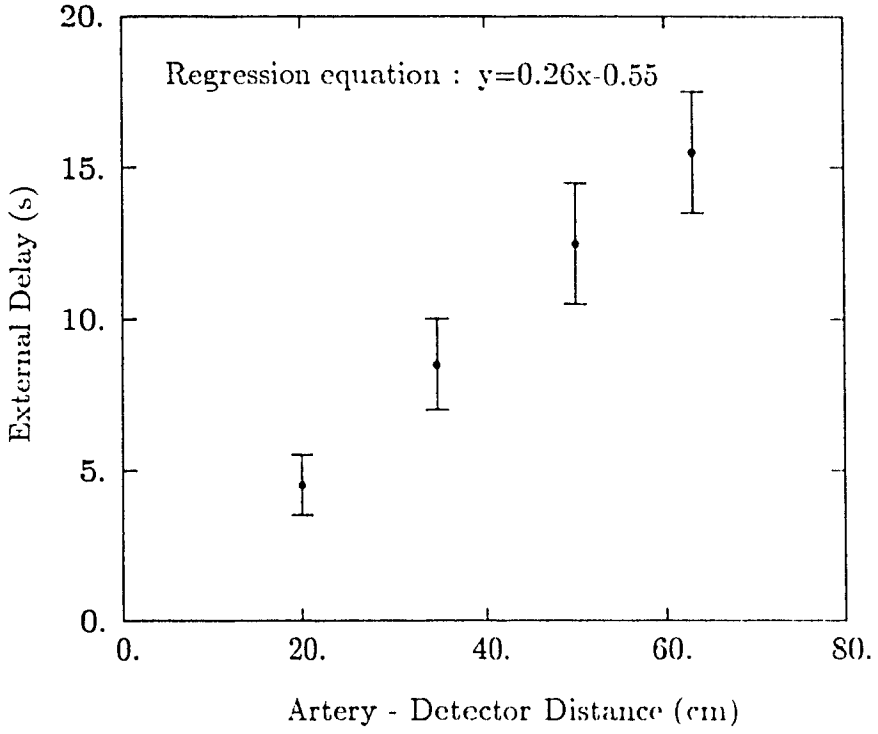

Figure 3.8 External delay vs. artery-detector distance of automated blood sampling system.

3.3.5.2 Delay by Least Squares Fitting

In order to verify the delay results obtained in the previous section, the following additional analysis was performed. Step response functions (see section 3.3.6) were fitted in two steps. First, the fitting was done for the flat part of the curve (representing the delay) up to the "breakpoint", N_x, where it starts to rise. Second, the rising part of the curve was fitted to the function 1-exp($-\frac{t}{\tau}$) using a dispersion time constant of τ=5.5 s (see next section) and the sum of least squares formed for both parts of the fit. This procedure was performed for a number of selected positions of the "breakpoint" N_x. The smallest sum of least squares was obtained when the N_x was chosen closest to the point where the response function started to rise. This analysis was performed on N=10 step response functions yielding an average delay of 4.65±0.65 s which, for an artery-detector distance of 20.0 cm, compares favourably with the physical delay measurements (4.5±0 5 s) explained in the previous section.

3.3.6 External Dispersion

The degree of distorsion in the curve shape of the input function due to the withdrawal catheter of the ABSS, called external dispersion, was determined as follows.

3.3.6.1 Dispersion Time Constant

Using a mixture of water and sugar with a viscosity of 2.8 centipoise (average blood viscosity) and Ga-68 EDTA as a tracer, the detector system response to a step input at time zero was measured (Fig. 3.9). According to equation (2.10), and using the dispersion function proposed by Iida et al. [44], this response becomes: $y = 1 - \exp(-\frac{t}{\tau})$

where τ is the dispersion time constant. This may be shown as follows:

If one considers g(t) as the measured response which can be expressed as the convolution of the input function $C_a(t)$ with the system impulse response function, d(t), i.e. $g(t)=C_a(t)*d(t)$ where theasterisk denotes the convolution operation. In order to determine the input function $C_a(t)$, the system impulse response must be measured. If a step function input, $C_{a_s}(t)$ is assumed, then $g_s(t) = C_{a_s}(t)*d(t)$. It can be shown that the derivative of $g_s(t)$ with respect to time is equal to the impulse response, d(t) i.e.:

$$\frac{dg_s(t)}{dt} = \frac{d(C_{a_s}(t) * d(t))}{dt} = \frac{dC_{a_s}(t)}{dt} * d(t) = \delta(t) * d(t) = d(t) \qquad (3.3)$$

where the Dirac-delta function, $\delta(t)$[1], is the derivative of the step input function. Therefore we obtain the step response function as:

$$g_s(t) = \int_0^t d(t)dt = \int_0^t \frac{1}{\tau} exp(-\frac{t}{\tau})dt = 1 - exp(-\frac{t}{\tau}) \qquad (3.4)$$

The dispersion time constant, τ, can be determined by non-linear least squares regression of the step response function. The required regression software was first tested by fitting simulated step response functions of the form described by equation (4.1), upon which 5% random Poisson noise had been superposed, and by comparing the resulting values of τ with those used in the simulation (Appendix III). The results of those tests are summarized in Table 3.3. The difference between τ_{theo} and τ_{fit} did not exceed 8%.

Step function experiments were then performed with the ABSS for various artery-detector distances, withdrawal flow rates and viscosities, and the dispersion time constant determined as described above.

---

[1] Dirac-delta function, $\delta(t)$, is defined as follows:

a) $\delta(x\text{-}x_0) = 0$ for $x \neq x_0$

b) $\int_{-\infty}^{+\infty} \delta(x\text{-}x_0)dx = 1$ for $x = x_0$

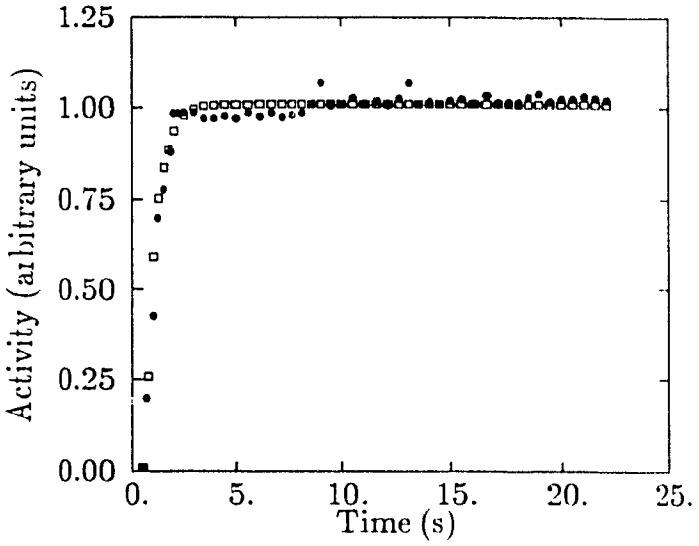

Figure 3.9 Step input response of the ABSS exhibiting the form 1-exp(-$\frac{t}{\tau}$) (• is the measured and □ is the fitted data).

Table 3.3 Dispersion time constants (τ) of simulated step response functions.

τ_{theo} (s)	τ_{fit} (s)
4.0	3.9±0.4 (96%)*
4.5	4.4±0.4 (97%)
5.0	4.9±0.4 (92%)
5.5	5.5±0.5 (99%)
6.0	6.1±0.6 (102%)
6 5	6.8±0.6 (105%)
7.0	6.9±0.6 (99%)

Values are means ± SD for n=10 experiments

* percentage of τ_{theo}

Figure 3.10 shows the expected increase of τ for increasing artery-detector distances which exhibits a linear behaviour. The dispersion time constant as a function of withdrawal flow rate is depicted in Fig. 3 11 and the results of these studies summarized in Table 3.4. Again, the demonstrated decrease of τ with increasing withdrawal rate is not surprising since, the larger the withdrawal rate, the shorter the travelling time in the catheter and hence, the smaller the distortion of the tracer bolus. As apparent from Fig. 3.12 and Table 3.5, the effect of changes in viscosity of the tracer carrying substance (e.g. blood) is insignificant over the range of viscosities expected in practice.

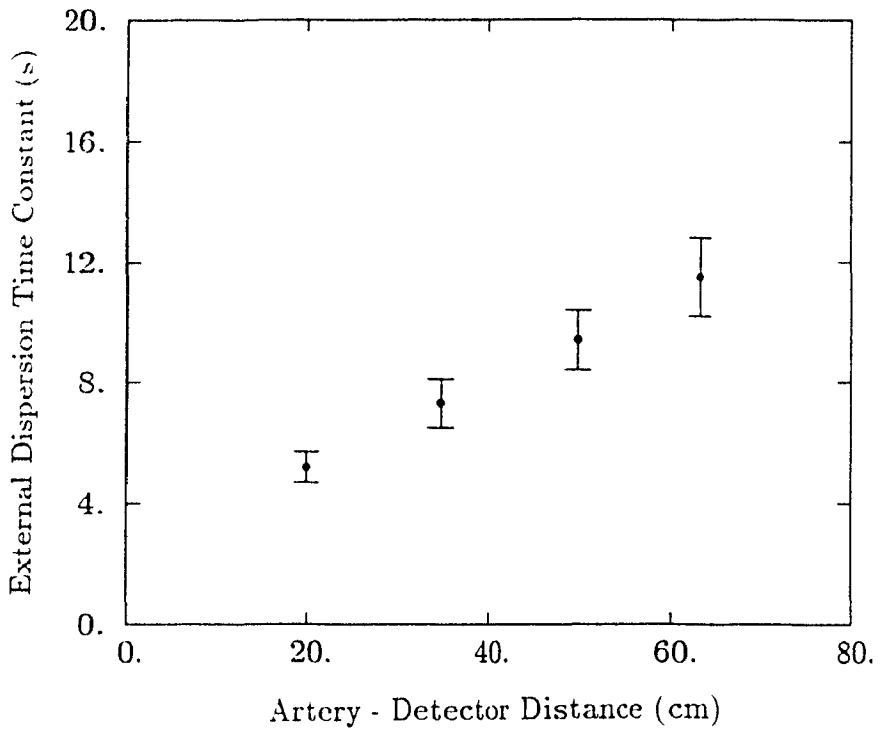

Figure 3.10 Effect of artery-detector distance on external dispersion time constant (τ).

Table 3.4 Effect of withdrawal rate on external dispersion time constant (τ).

Withdrawal flow rate ($ml \cdot min^{-1}$)	τ (s)
3.5	9.6± 0.9
5.5	6.9 ± 0.7
7.5	5.4 ± 0.5
9.5	3.5 ± 0.4

Values are means ± SD for n=15 experiments

Catheter length from detector to sampling site was 20 0 cm and viscosity of the solution was the same as average blood viscosity (3.0 centipoise)

Table 3.5 Effect of viscosity on external dispersion time constant (τ).

Viscosity (cp)	τ (s)
1.5	5.4± 0.8
3.0	5.4 ± 0.7
6.0	5.5± 0.7

Values are means ± SD for n=15 experiments

Flow rate was 7 5 ml min^{-1} and catheter length from detector to sampling site was 20 cm

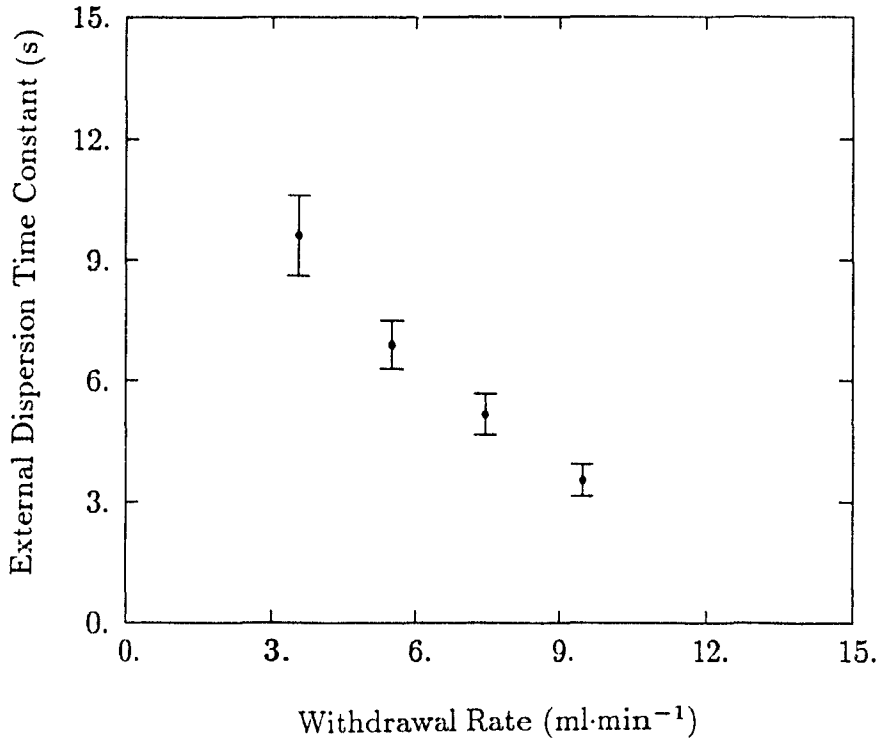

Figure 3.11 Effect of withdrawal rate on external dispersion time constant, τ.

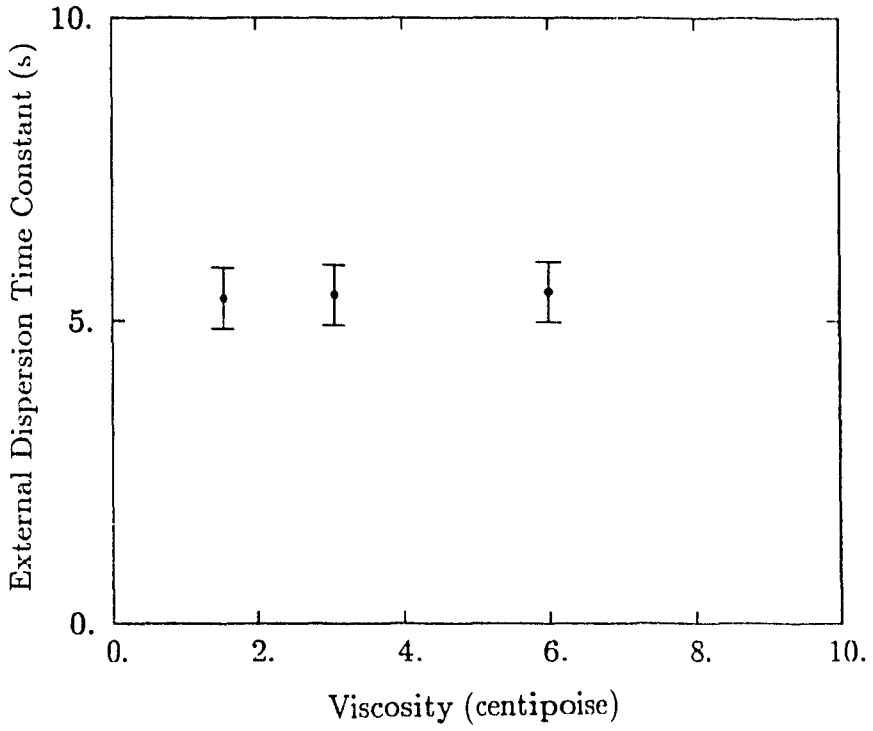

Figure 3.12 Effect of viscosity on external dispersion time constant, τ

In all experiments, a three-way stop cock was used at the sampling site (Fig. 4.1) in order to get blood samples both manually (from one end of the three-way stop cock) and automatically (from the other end). In practice, when automated sampling is performed exclusively, the three-way stop cock is replaced by a two-way connector. In order to check the effect of replacing the three-way connector with a two-way connector, step function experiments were performed to simulate 1) simultaneous manual and automated blood sampling and 2) automated sampling only. The results of non-linear least squares regression on these step response functions (determination of external dispersion time constant) showed that there was no significant difference between the two arrangements since τ differed by only 2%. This shows that the blood curves obtained with the three-way stop cock arrangement are reliable and may be compared with those obtained in practice when we use a two-way connector only.

CHAPTER 4

APPLICATION OF ABSS IN PATIENT STUDIES

After having verified the physical characteristics of the ABSS, such as linearity, external tracer delay and dispersion, it was used during PET CBF and CMR_{O_2} studies performed on volunteers. In the past, we had performed such studies with manual blood sampling exclusively. In order to assess the usefulness of the ABSS, the present studies were performed using manual and automated arterial blood sampling simultaneously. Using the manual curve as a reference, we then tried to match the two blood curves by applying a calibration plus corrections for radioactive decay as well as for external tracer delay and dispersion to the automated blood curve. The goodness of fit between the two curves was assessed by means of a chi-square test as well as by comparing their full widths at half maximum (FWHM).

In this chapter, we first briefly describe the PET CBF and CMR_{O_2} procedures during which the manual and automated blood data were collected. We then compare the manual and automated blood data sets and illustrate the effect of each of the above mentioned corrections.

4.1 Radioisotpe Preparation and Tomograph

The tracers $H_2{}^{15}O$ and $O^{15}O$ were prepared from a Japanese Steel Work

Baby Cyclotron BC-107. PET studies were performed on a Scanditronix PC-2048 15B, an eight-ring, 15-slice BGO head tomograph with a transverse resolution of 5.8 - 6 4 mm and an axial resolution of 6.1 - 7.1 mm. Its count rate efficiency was 9 7 Kcps/(μCi·ml^{-1}) for the direct slices and 13.7 Kcps/(μCi·ml^{-1}) for the cross slices [54] Reconstruction software included corrections for detector efficiency variations, random events and dead-time, as well as a deconvolution procedure to eliminate scattered events [55]. Attenuation correction was performed by means of an orbiting rod transmission source containing about 5 mCi of ^{68}Ge [54].

4.2 Subject Preparation

The subjects were positioned in the tomograph with their heads immobilized by means of a customized self-inflating foam headrest. A short indwelling catheter was placed into the left radial artery for blood sampling. A three-way stop cock (Fig. 4.1) was used to withdraw manual and automated samples. Manual samples were taken from one exit of the stop cock using a short (approx. 2 cm) catheter while blood was directed to the automated sampling system through a long (22 cm) catheter using the other exit of the stop cock. Although the external delay and dispersion characteristics of the ABSS have been standardized for a 20 cm long withdrawal catheter, the additional 2 cm of catheter

were used to compensate, with regard to delay and dispersion, for the short catheter (2 cm) used for manual sampling.

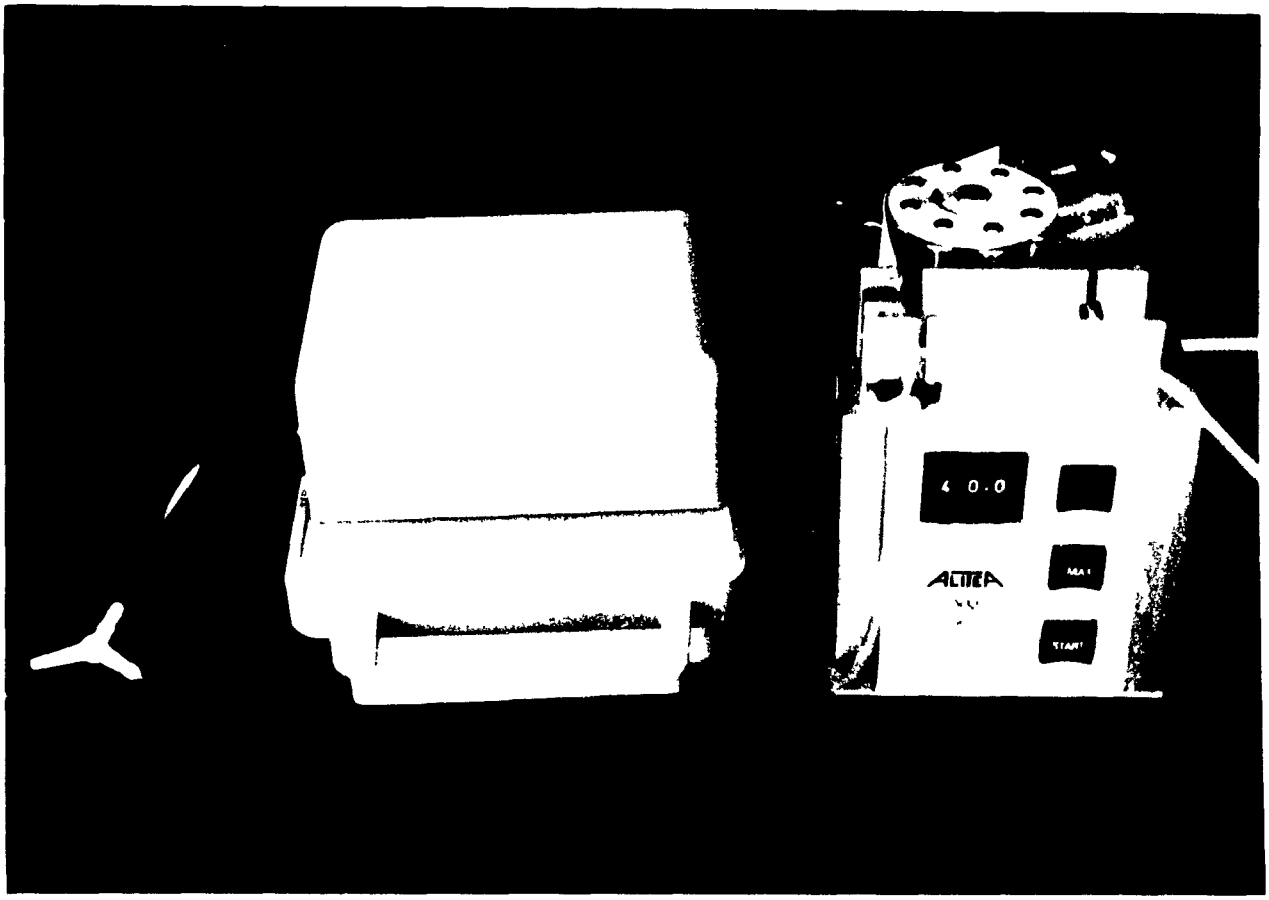

Figure 4.1 Set-up for manual and automated blood sampling using a three-way stop cock.

4.3 CBF Studies

Cerebral blood flow (CBF) was measured by the intravenous $H_2{}^{15}O$ bolus method [25,26] based on the one-compartment model outlined in chapter 2.

About 40 mCi of $H_2{}^{15}O$ were injected into the brachial vein of the right arm. Arterial blood sampling and dynamic imaging were started at injection time. Dynamic scans with frame durations of 5 s were obtained over a period of 3 min. Blood samples were collected both manually and with the ABSS. Manual sampling was initially performed at 3-5 s intervals which were gradually lengthened to 10 s and eventually 30 s towards the end of the data acquisition period where the blood activity varies slowly. Manual samples were assayed in a well-counter calibrated with respect to the tomograph, weighed and corrected for radioactive decay. Automatic blood sampling was performed at a continous withdrawal rate of 7.5 ml·min^{-1} and a sampling interval of 0.5 s throughout the data collection period. The automated blood sample count rate was recorded by the computer in counts per 0.5 s. In order to calibrate the automated blood curve with respect to the manual one, four calibration samples were collected from the very end of the withdrawal catheter where the blood is discarded into a waste basin (Fig. 4.2). The calibration procedure will be described in detail in paragraph 4.5.2. The remaining blood curve corrections will be explained and illustrated in section 4.5 of this chapter.

Figure 4.2 Detail of set-up for manual and automated blood sampling. The short catheter on the distal end of the three-way stop cock is used for manual sampling.

4.4 CMR_{O_2} Studies

CMR_{O_2} was measured by means of the single $[^{15}O]O_2$ bolus inhlation method of Ohta et al. [5]. In contrast to the CBF studies where $H_2{}^{15}O$ was administered by intravenous bolus injection, here, the tracer was administered by inhalation as follows: $[^{15}O]O_2$ was supplied from the cyclotron into a lead-shielded rubber bag at the subject's side where it was mixed with medical air. After a sufficient level of activity had accumulated, the subject, wearing a nose clamp, inhaled the gas (approx. 70-80 mCi) via a mouthpiece and a short connecting ventilator hose by taking a single deep breath and holding it for about 10 seconds. Scanning and blood sampling were initiatd at the start of inhalation while the manual and automated blood sampling were performed as described in the previous section.

4.5 Blood Data Corrections

Corrections for radioactive decay, external tracer arrival delay and dispersion due to the additional length of the sampling catheter in the ABSS are required to compare the blood data from the ABSS with the manually sampled data.

4.5.1 Radioactive Decay Correction

The automated blood data, which is very finely sampled at 0.5 s intervals, is corrected according to the expression $N(o) = N(t)\exp(\lambda \cdot t)$, where λ is the radioactive decay constant, N(o) the corrected activity with respect to time zero (injection time) and N(t) the uncorrected activity measured at time t. Figure 4.3 shows the automated blood curve before and after decay correction.

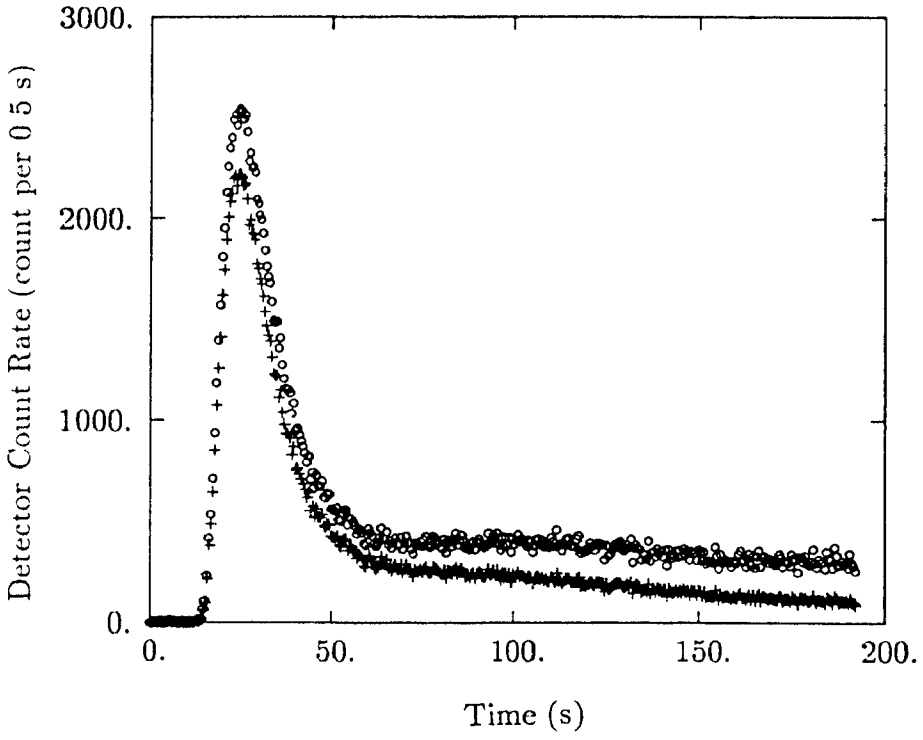

Figure 4.3 Automated blood curve before (+) and after (o) radioactive decay correction.

4.5.2 Calibration

Quantitative comparison of the manual blood data, usually given in units of cps·g^{-1}, with the automated data, given in cps, requires a calibration procedure. For this purpose, during each study, four blood samples are manually withdrawn from the distal end of the automated sampling catheter (where the blood is pouring into the waste container) and assayed in the same well counter as the manual samples. It is important to take these calibration samples during the flat part of the arterial curve where there is almost no change in blood activity. In this way, any possible sampling error (e.g. timing inaccuracy) will cause only a minor error in the calibration factor as illustrated in Fig. 4.4. For this reason, the calibration samples are usually taken two minutes after tracer administration. To find the calibration factor for each study, we rationalized that for each point y_i $(i = 1, \ldots, 4)$ on the manual curve (Fig 4.5), there is a corresponding point z_i $(i = 1, \ldots, 4)$ on the automated curve such that $Fz_i = y_i$ $(i = 1, \ldots, 4)$ where F is the calibration factor. To get the best value for F from the four calibration samples, we used a least squares optimization as follows.

$$\sum_{i=1}^{4}(Fz_i - y_i)^2 = \textbf{minimum} \tag{4.1}$$

Solving for F, we obtain:

$$F = \frac{\sum_{i=1}^{4} y_i z_i}{\sum_{i=1}^{4} z_i^2} \tag{4.2}$$

where the y_i's are counts from the manual samples assayed in the well counter [cps·g^{-1}] and the z_i's counts from the automated blood samples [cps]. Therefore, F, has unit of [g^{-1}]. Since, for our experimental condition (i.e. a sample withdrawal rate of 7.5 ml·min^{-1}), there is a sixteen second time difference between the detector site and the end of the sampling catheter where the calibration samples are taken, the point corresponding to y_1(t) is z_1(t-16s).

A computer program, called GET_CALBLD, which accepts the decay corrected automated blood curve as input and gives the calibrated automated blood curve as output was developed (see Appendix IV for program and calibration sheet).

Since the calibration samples are collected manually and therefore are subject to timing errors (start and stop sampling time), we investigated the sensitivity of F to such errors. For this purpose, F was first determined from the blood curves of five CBF studies as described above assuming no timing error (0 s error). A timing error of ±2 seconds was then applied to the calibration samples and F calculated again. Table 4.1 shows that, since the calibration samples are taken from the flat part of the blood curve, this timing error does not have

a big effect on F ($\sim \pm 2\%$).

It is important to realize that F may vary considerably from study to study (Table. 4.1, column 2). The fluctuations are most likely due to the temperature sensitivity of the radiation detectors, both in the ABSS and the well counter and the associated electronics. For an accurate quantification of CBF and CMR_{O_2} it is therefore mandatory to perform individual calibration for each study.

Table 4.1 Effect of sampling timing error on calibration factor, F.

Subject	F [g^{-1}]	ΔF [%]	
#	0 s error	+2 s error	-2 s error
1	48	+1.9	-1.6
2	55	+1.1	-1.9
3	58	+1.8	-1.2
4	59	+2.5	-2.5
5	63	+3.1	-3.3
mean		+2.1±0.4	-2.1±0.4

$p < 0.005$ by paired Student's t-test

Figure 4.6 shows a decay corrected, calibrated automated blood curve in comparison with a manual one. It is obvious from the figure that these two curves do not match yet. The remaining difference between the two curves is due to external tracer delay (shift along x-axis) and dispersion (peak height), which will be discussed next.

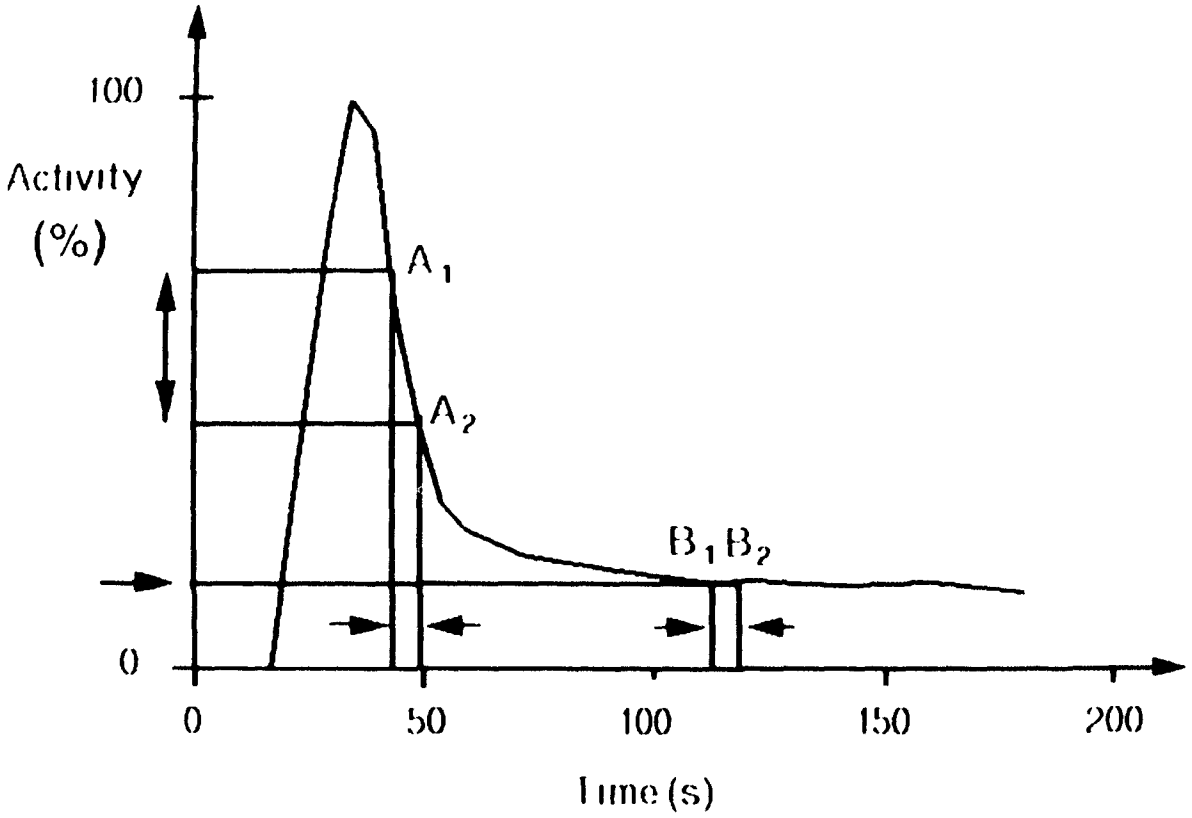

Figure 4.4 Illustration of the importance of choosing calibration samples in the flat part of blood curve. A small timing error in the peak part (points A_1 and A_2) will yield a large difference in blood activity and lead to a large error in the calibration factor, F.

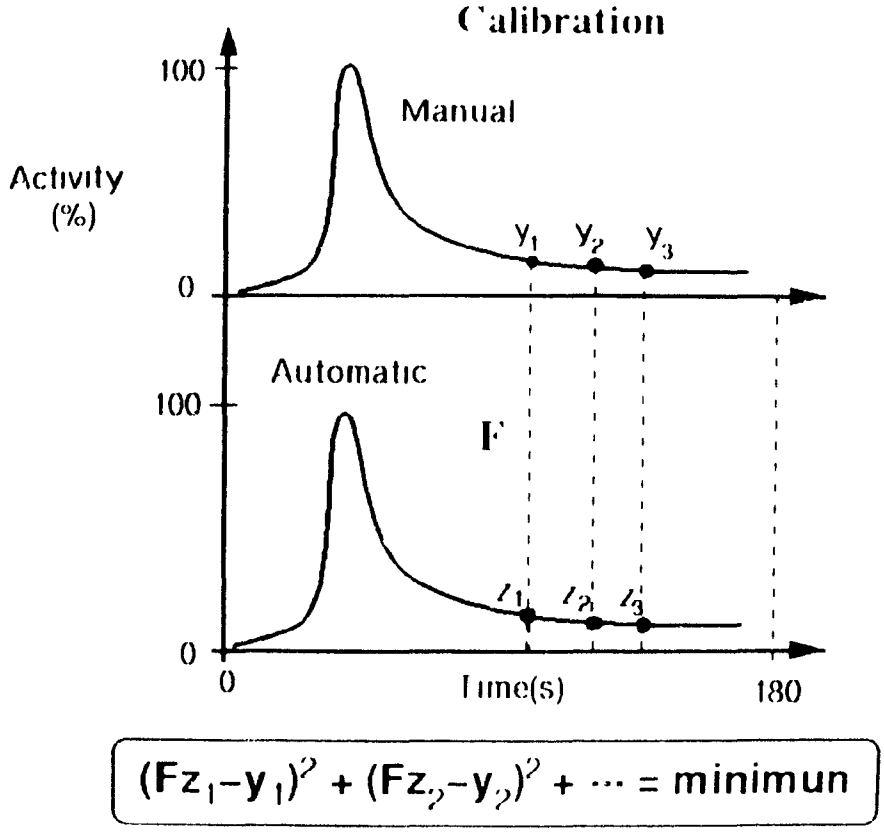

Figure 4.5 Procedure of calculating the calibration factor, F.

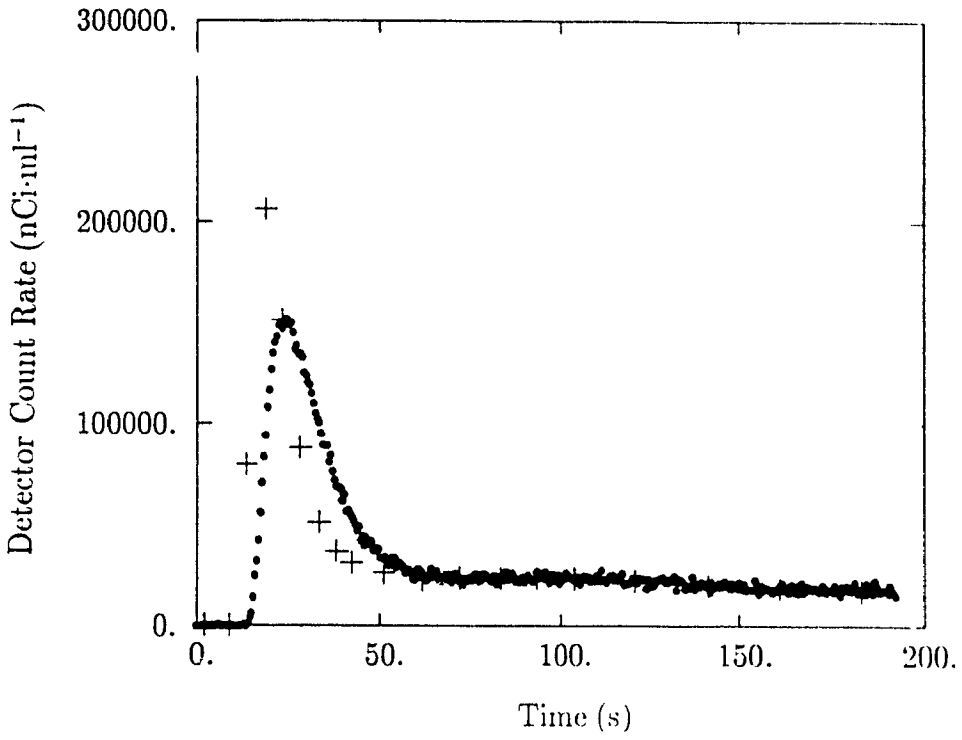

Figure 4.6 Comparison of a decay corrected and calibrated automated blood curve (•) with a manual one (+), also corrected for radioactive decay.

4.5.3 External Delay Correction

As explained in chapter 3, external delay is the time difference between the arterial site where blood is withdrawn and the mid-point of the coincidence detector pair where the blood tracer concentration is measured. The automated blood curve has to be corrected for this delay. Since, for the present study, the artery-detector distance of the ABSS was 20 cm and the withdrawal flow rate 7.5 ml·min^{-1}, we applied this correction by shifting the automated blood curve 4.5 s (Table 3.2) to the left on the time axis.

4.5.4 External Dispersion Correction

The correction for the difference in the degree of distortion between the curve shape of the manual ($C_a(t)$) and the automated ($g(t)$) input function, resulting from the dispersion of the tracer bolus in the additional length of sampling catheter, is called external dispersion correction. As shown in chapter 2 (equation 2.10), the relation between $C_a(t)$ and $g(t)$ can be written as:

$$g(t) = C_a(t) * d(t) \tag{4.1}$$

where the asterisk means the convolution operation[3] and d(t) is the dispersion function. Various models have been proposed to perform this correction [44,35,43]. We adopted the monoexponential model proposed by Iida et al. [44],

[3]The convolution, h(t), of two functions x(t) and y(t) is defined as: $h(t)=\int_{-\infty}^{+\infty} x(\tau)y(t-\tau)d\tau$.

whose dispersion function is:

$$d(t) = \frac{1}{\tau} exp(\frac{-t}{\tau}) \qquad (4.2)$$

With this model, the true input function may be recovered from the measured blood data using Laplace transforms [33,44] as follows:

$$C_a(t) = g(t) + \tau(\frac{dg}{dt}) \qquad (4.3)$$

where τ is the external dispersion time constant which has been experimentally determined in chapter 3 (Table 3.3 and Fig. 3.11).

We have developed a program (GET_DELCONSMO, Appendix V) to perform the deconvolution according to eq. 4.3. It accepts the decay corrected and calibrated automated blood curve as input and gives the deconvolved blood curve as output for a given dispersion time constant, τ. For an artery-detector distance of 20 cm and a withdrawal flow rate of 7.5 ml·min^{-1}, which are standard for our ABSS, an average value of τ = 5.5 s was used (Fig. 3.11 and Tables 3.4 and 3.5). This program GET_DELCONSMO also performs the external delay correction discussed in the previous paragraph. In order to reduce the statistical noise on the curve, brought about by the derivative in equation 4.3, a parabolic smoothing filter was used [56]. With this method, a function of the form $y_k = a + bk + ck^2$ is fitted to consecutive data values over a selected odd number of n points, symmetrically disposed about the point for which k =0.

The value of the best-fit parabola at k=0 (i.e. $y_0 = a$) is taken as the smoothed value of the data for that center point. This operation requires the three best-fit coefficients a,b,c which in term provide the smoothed data value, y_k, the slope and the rate of change of the slope, respectively. The precise nature of the filter is dependent upon the number of points, n, over which the parabola is fitted. The larger the value of n, the heavier the smoothing of the data, and vice versa.

Figure 4.7 shows an automated blood curve before and after deconvolution. It is apparent that the peak of the dispersion corrected (deconvolved) curve is higher and shifted towards the left (earlier times) with respect to the non-corrected one. In Figure 4.8, the effect of the parabolic smoothing filter on a dispersion corrected automated blood curve is shown. In order to minimize any distortion in the peak region, in particular to avoid a significant reduction in peak height, the first 50 s of the curve were smoothed only lightly, using a value of $n = 5$. From there on, the flat section of the curve was smoothed more heavily with a value of $n = 19$. Figure 4.9 shows that a perfect match between a smoothed, calibrated automated blood curve and the corresponding manual one can be obtained, provided the appropriate corrections for radioactive decay, external delay and dispersion have been applied.

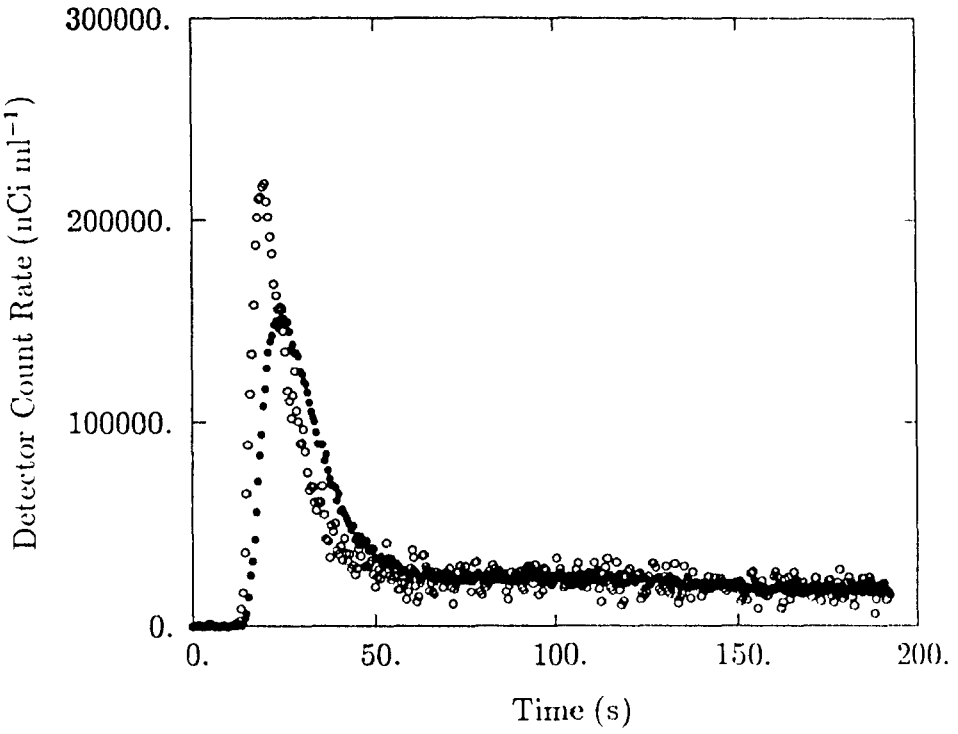

Figure 4.7 An automated blood curve before (•) and after (o) dispersion correction (deconvolution).

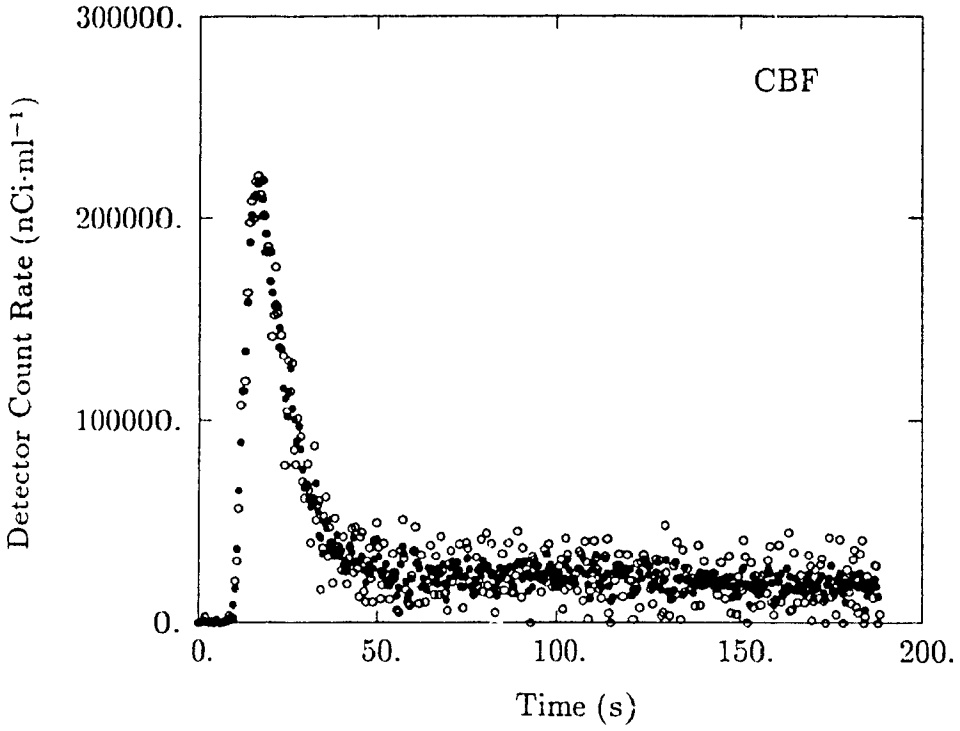

Figure 4.8 Comparison of a smoothed (•) and unsmoothed (○) dispersion corrected (deconvolved) automated blood curve.

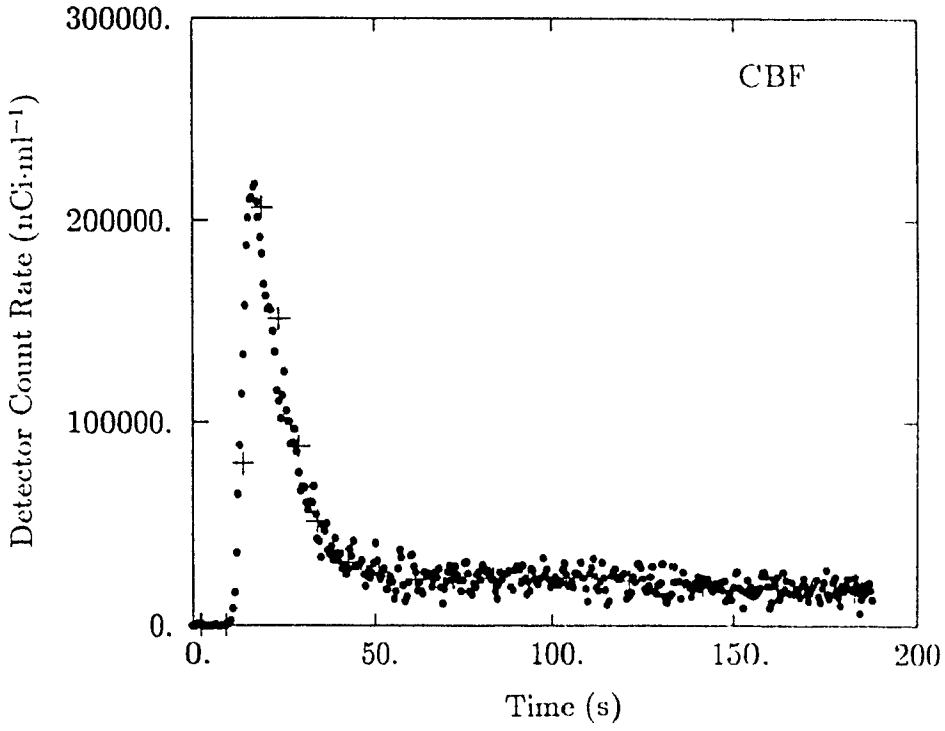

Figure 4.9 Comparison of a decay, delay and dispersion corrected smoothed automated blood curve (•) with the corresponding manual one (+). Note the excellent match of the two curves.

4.5.5 Comparison of Blood Data

While Fig. 4.9 provides a qualitative comparison of the manual and automated blood data, a quantitative comparison was performed by means of a goodness of fit analysis using the chi-square (χ^2) test with the manual blood curve as a reference as well as by an evaluation of the full width at half maximum (FWHM) of the peak of the input function. For this purpose, the manual blood data were interpolated based on the time scale of the automated curve. The goodness of fit analysis on seven blood curves from O-15 water CBF studies yielded χ^2 values ranging between 5.1×10^{-6} and 4.9×10^{-5}, indicating an excellent match between the two data sets. The comparison of their FWHM values by means of a paired Student's t-test, however, showed a small, but statistically significant difference (Table 4.2).

Applied to seven blood curves from $[^{15}O]O_2$ CMR_{O_2} studies, using the same correction parameters as in the CBF studies, the goodness of fit analysis yielded significantly larger χ^2 values ranging between 3.8×10^{-4} and 2.9×10^{-3} (Table 4.2), indicating some degree of discrepancy between the manual and automated data sets. In order to get a better fit, the dispersion time constant was varied between 4.0 and 8.0 s and the resulting curves were again compared with the manual ones by calculating the corresponding χ^2 values. The smallest χ^2 value was found for a dispersion time constant of $\tau = 7.0$ s. Also, the FWHM

analysis of the $[^{15}O]O_2$ blood curves showed a persisting mismatch between the manual and automated data sets (Table 4.4). This interesting difference between the behavior of the blood data from the CBF and CMR_{O_2} studies, which might be linked to the difference in the labeled fractions of the blood for the two tracers, will be discussed in more detail in chapter 6.

Table 4.2 Results of chi-square test between manual and automated blood curves for CBF and CMR_{O_2} studies

Subject	χ^2_{CBF}	$\chi^2_{CMR_{O_2}}$
1	5.1×10^{-6}	3.8×10^{-4}
2	6.4×10^{-6}	5.1×10^{-4}
3	7.3×10^{-6}	5.7×10^{-4}
4	7.8×10^{-6}	6.3×10^{-4}
5	3.2×10^{-5}	1.1×10^{-3}
6	2.9×10^{-5}	2.3×10^{-3}
7	4.9×10^{-5}	2.9×10^{-3}
mean	1.9×10^{-5}	120×10^{-5}

Results were obtained with external tracer delay (Δt) of 4.5 s and external dispersion time constant (τ) of 5.5 s

Table 4.3 Comparison of FWHM for automated and manual blood curves used to obtain CBF images.

#	$FWHM_{aut}[s]$	$FWHM_{man}[s]$	Difference* [%]
1	10	11	9
2	16	17	5
3	12	12	0
4	13	13.5	3
5	18	18.5	2
6	15	16	6
7	14	15	7
mean	14.0±0.9	14.6±0.9	4.5±0.5

$p < 0.005$ by paired Student's t-test

* $\frac{FWHM_{man}-FWHM_{aut}}{FWHM_{man}} \cdot 100$

Table 4.4 Comparison of FWHM for automated and manual blood curves used to obtain CMR_{O_2} images.

#	$FWHM_{aut}[s]$	$FWHM_{man}[s]$	Difference* [%]
1	18	22	18
2	22	30	26
3	20	28	28
4	14	20	30
5	22	26	15
6	22	26	15
mean	19.6±3.2	25.3±3.7	22 0 1.6.78

$p < 0\ 0009$ by paired Student's t-test

* $\frac{FWHM_{man}-FWHM_{aut}}{FWHM_{man}} \cdot 100$

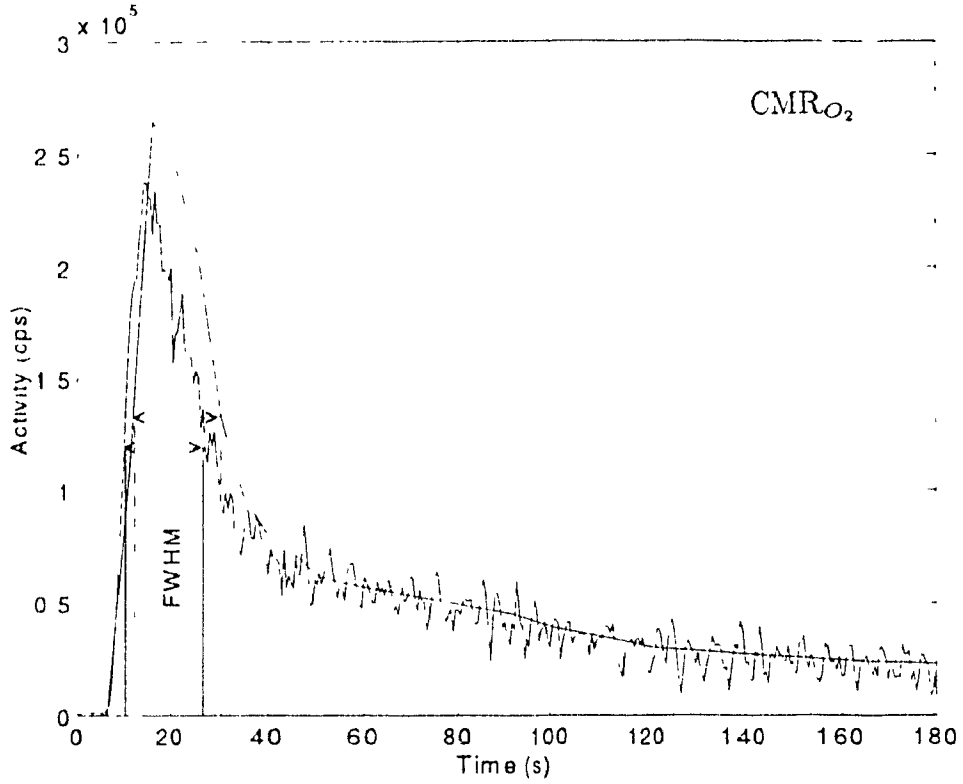

Figure. 4.10 Comparison of FWHM for automated and manual blood curve from CMR_{O_2} study.

CHAPTER 5

CBF AND CMR_{O_2} RESULTS

Following application of the required corrections to the automated blood curves, which were discussed in the previous chapters, both the corrected automated and the manual curves were used to analyze a series of CBF and CMR_{O_2} PET studies that were performed on young normal volunteers as part of an ongoing research project. The resulting CBF and CMR_{O_2} pairs were compared in order to assess the reliability and degree of equivalence of the two blood sampling methods.

5.1 CBF Results

Cerebral blood flow images were generated from positron emission tomographic data (Fig. 5.1) as described by Herscovitch et al. [25] and Raichle et al. [26], using the global fitting method for internal delay correction [43]. No correction for internal dispersion was applied since, at a sample withdrawal flow rate of 7.5 $ml \cdot min^{-1}$, this effect has been shown to be minimal [44]. Functional values were calculated for all fifteen simultaneous slices produced by the tomograph and the results averaged in order to get the mean whole brain blood flow for seven healthy volunteers, using both manual and automated blood data (Table 5.1). Comparison of the results from this study showed that, on aver

age, the CBF values obtained with automated blood sampling were consistently higher (+4%) than those obtained with manual sampling. This difference was significant at $p<0.0001$ by Student's paired t-test. Individual CBF values from automated blood data, in general, exceeded those based on manual data by no more than approximately 5%.

One might be tempted to attribute the observed discrepancy between the two results to the fact that manual blood sampling requires recording of the start and stop time for blood sample collection and, therefore, is error prone. It is well known that timing errors as small as 1 s in the blood data result in CBF errors of almost 10% [25]. This fact is illustrated in Table 5.1 which summarizes the error in CBF due to a ± 2 second timing error in the blood data (Fig. 5.1) However, since this timing error is expected to occur randomly and since the corresponding CBF error assumes both positive and negative values, the observed consistent overestimation of CBF_{man} by CBF_{auto} (Table 5.2) is more likely related to the observation that the FWHM of the manual blood curve is slightly, but significantly, wider than that of the automated one (Table 4.2). This widening is most likely due to the limited timing resolution of the manual blood curve as opposed to the automated one (see chapter 6 for a more detailed discussion). Therefore, we may conclude that, since the automated blood sampling system can record data every half second, the CBF values obtained

from the automated blood curves are more reliable than those derived from the manual ones.

Table 5.1 Percentage error in whole brain CBF values resulting from manual blood curves with a ± 2 s sample timing error

Subject	ΔCBF [%]	
#	+2 s error	-2 s error
1	+5.3	-6.6
2	+8.1	-6.3
3	+7.3	-9.0
4	+5.5	-8.5
5	+6.1	-7.8
mean±SD	+6.5±1.2	-7.6±2.3

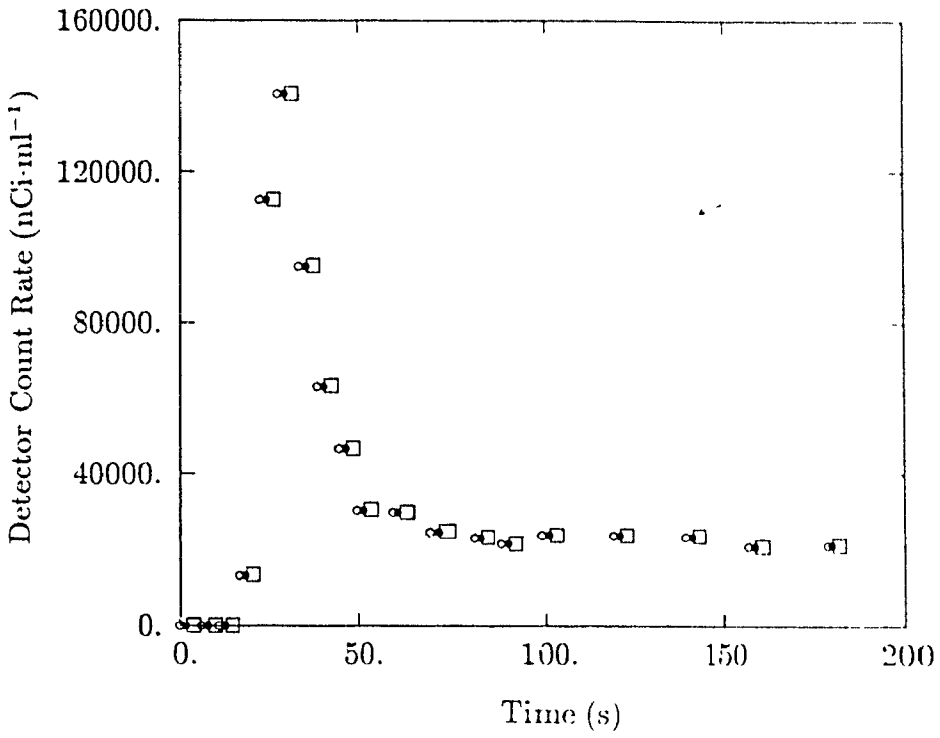

Figure 5.1 Manual blood curve with a timing error of +2 s (□) and -2 s (○) (• is the original curve).

Table 5.2 Whole brain CBF values ($ml \cdot hg^{-1} \cdot min^{-1}$) obtained from seven young volunteers using automated and manual blood data.

subject #	CBF_{aut}	CBF_{man}	$\frac{CBF_{aut}-CBF_{man}}{CBF_{man}} \cdot 100[\%]$
1	30.8± 10.5	29.3± 9.5	+5.1
2	49.1± 13.2	48.2± 12.3	+1.8
3	34 3± 9.8	33.2± 9.7	+3.3
4	34.2± 9.6	32.1± 9.4	+3.3
5	40.1± 12.3	38.1± 15.6	+5.2
6	37.1± 9.9	35.2± 9.7	+5.3
7	54.5± 8.9	52.3± 8.7	+4.2
mean	40.0±8.7	38.3±8.6	+4.0±1.2

Values are means ± SD

$p < 0.0001$ by paired Student's t-test

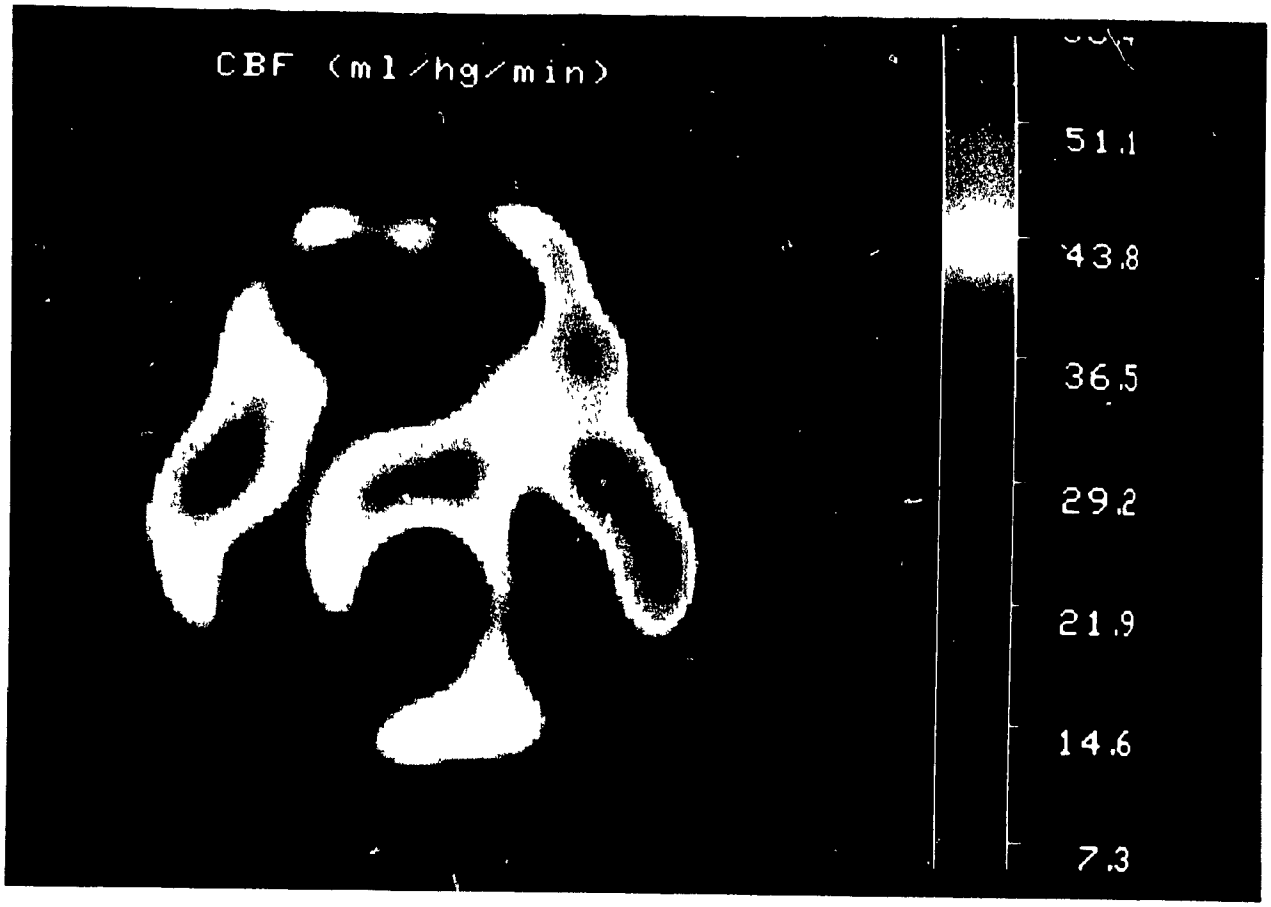

Figure 5.2 Example of a CBF image of one brain slice from a young volunteer generated from automated blood data.

5.2 CMR_{O_2} Results

CMR_{O_2} images from seven healthy volunteers were obtained using the three-weighted integration method of Ohta et al. [5] (Fig. 5.3). Mean whole brain cerebral oxygen metabolic rates were calculated for all fifteen simultaneous slices, using manual and automated blood data, and the results were compared. This comparison showed that the CMR_{O_2} values obtained with the automated data were consistently more than 20% higher than those obtained with the manual blood data. Excluding the manual blood data timing uncertainty as a major cause for this result, for the same reason as discussed in the previous paragraph, we identified two causes which might explain our observation. First, we noticed that dispersion correction with the same time constant as in the CBF studies (τ = 5.5 s) did not allow to properly match the manual and the automated blood curves. In particular, the peak heights of the automated curves consistently failed to reach those of the manual ones. Gradually increasing the external dispersion time constant reduced the discrepancy between the manual and the automated CMR_{O_2} which, for τ = 7.0 s, reached a minimum of approximately 12%, but did not vanish (Table 5.3). The remaining difference therefore, was again attributed to the discrepancy in the FWHM between the manual and the automated blood curves which was much more important here than in the CBF studies (Table 4.3). This issue will be discussed in chapter 6.

Table 5.3 Whole brain CMR_{O_2} values (μmol·hg^{-1}·min^{-1}) obtained from seven young volunteers using automated and manual blood data.

subject #	$CMR_{O_2 aut}$	$CMR_{O_2 man}$	$\frac{CMR_{O_2 aut} - CMR_{O_2 man}}{CMR_{O_2 man}} \cdot 100[\%]$
1	168.1± 60.5	152.3± 59.5	+10 3
2	166.8± 65.1	152.3± 63.4	+9 5
3	140.1± 60.3	128.3± 57.8	+9.1
4	139.2± 58.3	127.1± 55 5	+9 5
5	145.5± 49.9	130.3± 48.7	+11.6
6	155.5± 59.9	143.5± 52.3	+8.3
7	150.5± 55.5	134.1± 50.5	+12.2
mean	152.2±11.8	138.3±11.0	+10 1±2.3

Values are means ± SD

p < 0 00006 by paired Student's t-test

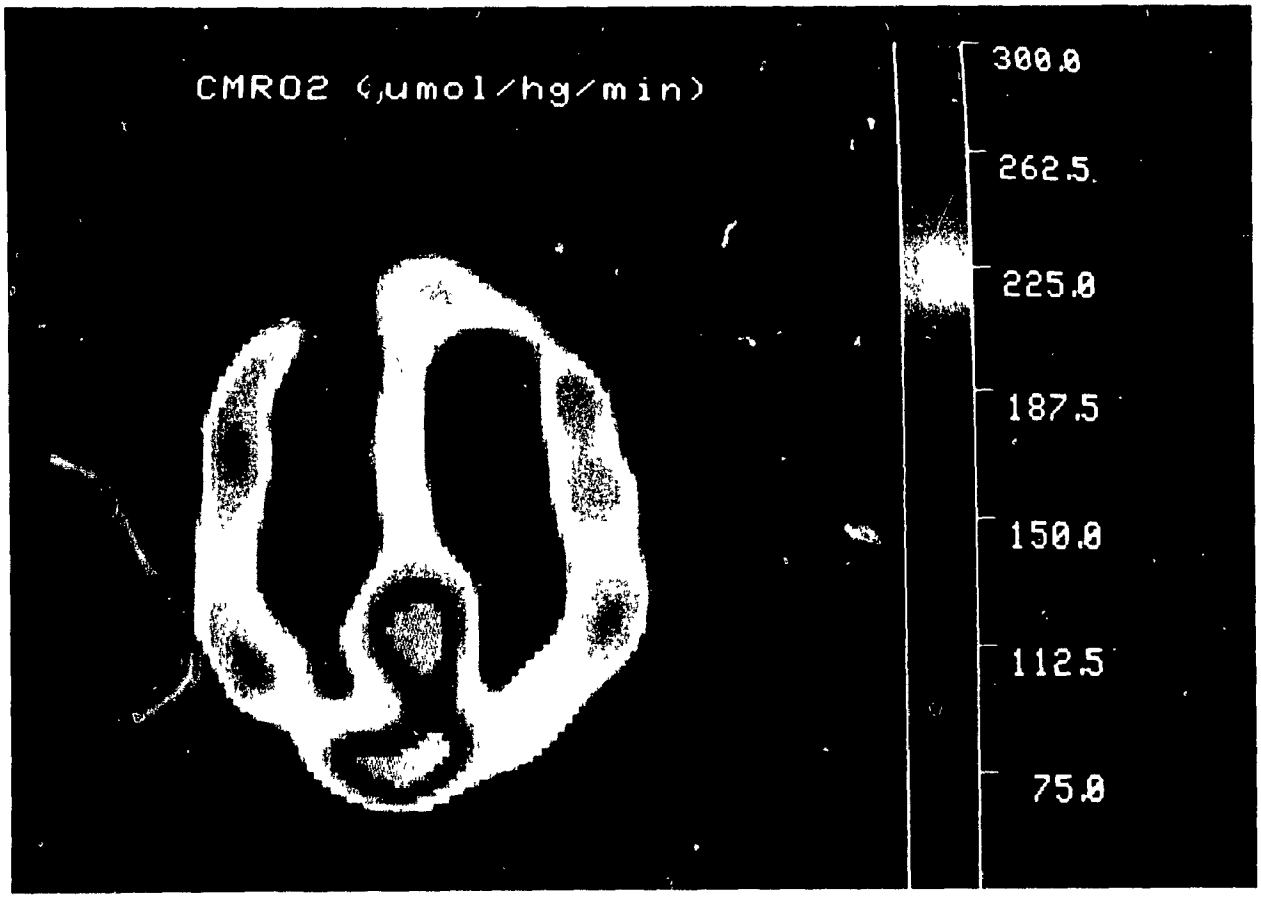

Figure 5.3 Example of a CMR_{O_2} image of one brain slice from a young volunteer generated from automated blood data.

CHAPTER 6

DISCUSSION AND CONCLUSIONS

Positron emission tomography allows the in-vivo investigation of a variety of physiologic[al] [and] physiological processes. Their quantification in terms of measurable [parameters] such as CBF requires the knowledge of the arterial concentration [of the tracer] and its eventual metabolites. In most instances, but particularly during dynamic studies where the tissue radioactivity is recorded as a function of time, rapid sampling of the arterial input function is required since tracer administration is frequently performed as a bolus injection which results in a rapidly changing initial phase of the arterial tracer concentration. In addition, most positron emitting radioisotopes are relatively short-lived with oxygen-15, the most frequently used tracer for CBF measurements, having a half-life of only 2 min.

The use of automated blood sampling during such studies has a number of advantages. First, the sampling time interval can be reduced from the practical manual limit of approximately 3 to 5 s to a fraction of a second which allows a more faithful recording of the true shape of the arterial input function Second, the accuracy of automated timing is superior to that obtained by the manipulation of a stopwatch. Furthermore, a single individual can perform the automated blood sampling with minimal manual intervention and, therefore,

reduced exposure to radiation. Properly tested automated blood sampling systems also facilitate the routine performance of a number of PET investigations which are more and more frequently seen in clinical applications [14,15,23].

The disadvantage of such blood sampling systems, however, consists in the external sampling catheter which extends from the manual sampling site to the external radiation detector. This necessitates an additional correction for tracer arrival delay and dispersion, termed external delay and dispersion, as opposed to the delay and dispersion incurred by the tracer in the blood vessels of the body between the heart and the brain on the one hand and between the heart and the peripheral manual sampling site on the other hand. Most physiological parameters derived from PET studies are sensitive to errors in these corrections, particularly estimates of quantities related to the intravascular space such as the initial vascular distribution volume of water [5].

The approach we chose for the evaluation and implementation of the Scanditronix ABSS is based on a comparison of the manually sampled blood data with that obtained with the ABSS using data from PET CBF and CMR_{O_2} studies during which manual and automated blood sampling was simultaneously performed. Our aim was to demonstrate that, after application of the appropriate corrections for external delay and dispersion, the manual and automated blood curves were practically equivalent, i.e., exhibited similar shapes

and yielded comparable CBF and CMR_{O_2} results. In order to validate such a comparison, we carefully verified that the simultaneous manual sampling did not affect the automated blood data (see chapter 3).

This approach was chosen to allow us to provide PET investigators with blood data they could use with existing analysis software tailored to manual blood data. A less flexible although more comprehensive approach would have been to incorporate the total (including the internal and external components) tracer delay, Δt, and dispersion time constant, τ, directly into the respective model equations as fitting parameters [34,42,]. This would have required the modification and retesting of the analysis software for each individual PET model (e.g. the CBF, CMR_{O_2} and CBV models, etc.). Furthermore, this approach might fail if the number of fitting parameters becomes too large (e.g larger than about 4).

A positive aspect of the Scanditronix ABSS is its coincidence detection design which results in a very low background count rate (less than 1%), an important feature considering the large source of background radiation represented by the radioactivity distributed in the body of the subject undergoing the

PET study One aspect of the Scanditronix ABSS, however, which we consider to be suboptimal is the use of a peristaltic pump for th withdrawal of blood. In our experience, such a pump requires extreme care to guarantee a constant withdrawal rate, and we have shown that Δt and τ depend very critically on the blood withdrawal rate. We would therefore recommend the use of the more reliable syringe withdrawal pump type already used in other laboratories [33,35].

For practical reasons, rather than using blood labelled with the short-lived tracer ^{15}O ($T_{1/2}$=2.03 min), we chose to investigate the physical characteristics of the ABSS, such as its linearity as well as its external delay and dispersion, by means of a water-sugar solution with the same average viscosity as that of blood and labeled with the longer-lived positron emitter Ga-68 ($T_{1/2}$=68.3 min).

We found that our ABSS exhibited excellent linearity in the practically expected range of blood radioactivity concentrations (Fig. 3.7). Also, our manual calibration procedure designed to make the automated blood data (cps) compatible with the manual data ($cps \cdot g^{-1}$) proved to be extremely insensitive to timing errors due to the judicious selection of the calibration samples from the later, relatively flat portion of the blood curve.

One of the important correction parameters, namely the external tracer delay, Δt, between the arterial sampling site (usually the radial artery) and the position of the radiation detector, was determined in three ways: 1) by means of

a calculation based on the physical dimensions of the withdrawal catheter, the artery-detector distance as well as the withdrawal flow rate (equation 3.2), 2) by measuring the transit time of the test fluid between the arterial sampling site and the position of the radiation detector; 3) by fitting a step response function to a step input experiment as described in paragraph 3.3.5.2 (the step input was achieved by manually dipping the proximal end of the withdrawal catheter into a beaker of radioactive solution at time zero). Comparison of the results from these three determinations showed agreement within 1% between the measured (4.50±0.50 s) and fitted (4.65±0.65 s) values while the calculated delay was about 10% larger (4.98 s), probably due to fluctuations in the catheter diameter or inaccuracies in its determination (note that the calculated delay is proportional to the square of the catheter diameter). We chose the physically measured value of 4.5 s as the standard delay correction for a fixed 20 cm artery detector distance and a withdrawal flow rate of 7.5 ml·min^{-1}.

For the description of the external dispersion, a simple monoexponential model with the dispersion time constant, τ, as the only parameter [44] was found to be satisfactory for $H_2{}^{15}O$ blood curves from CBF studies. The dispersion time constant was determined from step response functions by means of non linear least squares fitting and using the method of Laplace transforms to recover the "undispersed" (i.e. no external dispersion component) input function from the

dispersed (automated blood curve) one by means of deconvolution. This procedure required the derivative of the dispersed input function (equation 4.3) which introduced a significant amount of noise to the result. A parabolic regressive filter was therefore used to smoothe the deconvolved automated blood curve which facilitated the visual comparison with the manual one. Particular care was taken not to distort the peak height of the curve by smoothing the peak area only very lightly while applying a much stronger degree of smoothing to the flatter portion of the curve (time-variable filtering).

Another approach to this deconvolution problem would have been the use of Fourier transforms. This avenue, however, was not explored here due to time constraints.

The non linear least squares fitting program was tested on simulated noisy step response functions with known values of τ. For this purpose, the generation of random variables (or deviates) by means of a random number generator was used. Since such simulations are essential in many areas of PET-related research, we dedicated a fair amount of time to this subject (see section 3.3.4).

Analysis of the dispersion time constant studies showed that τ decreased approximately linearly with increasing withdrawal flow rate and decreasing artery-catheter distance. This behaviour would be intuitively expected. The dispersion correction factor, therefore, becomes minimal for the largest affordable blood

withdrawal flow rate and the shortest physically feasible artery detector distance. Based on these observations, we chose to operate the ABSS for a fixed set of parameters which included a relatively large withdrawal flow rate of 7.5 $ml \cdot min^{-1}$ (which is roughly the same as that previously used with manual sampling) and an artery detector distance of 20 cm. In this case, the external delay is 4.5 s and the dispersion time constant 5.5 s.

Since the blood viscosity may vary from subject to subject, particularly in certain diseases such as polycythemia vera, we measured the dependence of τ on the viscosity of the water-sugar solution. Within the expected clinical range of viscosities, this dependence was found to be negligible. Since real blood is not a Newtonian fluid, as opposed to water, and therefore exhibits different viscosity characteristics, one might want to repeat the latter experiment with blood as the test fluid in order to confirm our observation.

For the comparison of the calibrated, delay and dispersion corrected, automated blood curve with the manual one, we chose to perform a χ^2 test, using the manual curve as a reference. The χ^2 value is essentially a normalized sum of least squares which gets smaller, the better the fit, and vice versa. We further used the FWHM of the peak of the two curves as a means of comparison.

In the case of $H_2{}^{15}O$ blood curves from CBF studies, the two curves matched

very closely (Fig. 4.9). We attribute the slightly but consistently wider FWHM of the manual curve (Table 4.3) to the larger manual sampling interval which does not allow to recover the true blood curve shape with the same accuracy as the ABSS which has a 0.5 s sampling interval. The slightly higher CBF values (4%) obtained with the automated blood curves is consistent with this observation since, for a given tissue time-activity curve, the narrower the blood curve, the larger the corresponding CBF value. The possibility that a manual timing error might be the cause for this 4% difference was ruled out on the grounds of its random nature which would have lead to positive and negative fluctuations. The average CBF values derived from both blood curves agree well with literature values from similar PET studies [6]. Based on the above arguments, we conclude that the quantification of $H_2{}^{15}O$ bolus CBF studies using blood data collected with the Scanditronix ABSS is accurate and reliable.

When comparing the blood curves from the $O^{15}O$ CMR_{O_2} studies, the χ^2 values were substantially larger than in the CBF case (Table 4.2). Also, the discrepancy between the two FWHM measurements was more pronounced (Table 4.4). This led to CMR_{O_2} estimates which were 20% larger when calculated from the manual curves. Even when the dispersion time constant was arbitrarily increased from the standard value of 5.5 s to 7 s, which gave a somewhat better match of the two blood curves, a discrepancy of approximately 12 % remained

between the two CMR_{O_2} estimates. However, both values were within the range of accepted average CMR_{O_2} values [6].

This important remaining difference could not be explained by the different length of the blood sampling intervals, and we had to look for a more plausible reason. One explanation we considered was based on the fact that, unlike in the CBF studies where the tracer $H_2{}^{15}O$ is quite uniformly distributed between red blood cells and plasma, in the CMR_{O_2} studies with $O^{15}O$ as a tracer, red blood cells are exclusively labeled due to the high affinity of molecular oxygen for hemoglobin. It is known [57] that the flow patterns of red blood cells and plasma may differ substantially, particularly in vessels with diameters of 1mm or less. Under such conditions, significant hematocrit fluctuations may also occur which further complicates the issue. Since the correction parameters Δt and τ were derived from a uniformly labeled aqueous solution flowing through a catheter with an inner diameter of approximately 1mm, it is not surprising that they do not exactly apply to the case of non-uniformly labeled blood. Therefore, when τ was artificially increased, the manual and automated blood curves more closely resembled each other. The remaining difference in shape might be related to a combination of effects due to the different flow patterns of plasma and red blood cells as well as to possible hematocrit effects. This intriguing phenomenon, therefore, deserves further investigation

The important conclusion to be drawn from these observations is that, in order to avoid significant quantification errors in the analysis of PET studies, the external delay and dispersion characteristics of automated blood sampling systems should be evaluated individually for each tracer rather than derived from tests with uniformly labeled radioactive solutions [58]. If this is not possible for practical reasons, effects related to the proportioning of the label between the plasma and red blood cell fractions have to be carefully examined. In fact, even the slight discrepancy in the CBF studies might be due to the known, although small, difference in the fractional water contents of whole blood (0.80 g per g-blood) and plasma (0.92 g per g-plasma) [47].

In summary, then, we may say that we have successfully implemented the Scanditronix ABSS for routine use in quantitative $H_2{}^{15}O$ bolus CBF studies.

LIST OF FIGURES

Figure 3.4 Pumping system with withdrawal catheter.

Figure 3.5 Automated blood sampling system including detector, pump and catheter.

Figure 3.6 Performance of pumping system at withdrawal rates of 9.5 (□), 7.5 (•), 5.5 (▪) and 3.5 (o) ml·min^{-1}.

Figure 3.7 Linearity test of automated blood sampling system.

Figure 3.8 External delay vs. artery-detector distance of automated blood sampling system.

Figure 3.9 Step input response of the ABSS exhibiting the form 1-exp(-$\frac{t}{\tau}$) (• is the measured and □ is the fitted data).

Figure 3.10 Effect of artery-detector distance on external dispersion time constant (τ).

Figure. 3.11 Effect of withdrawal rate on external dispersion time constant, τ.

Figure 3.12 Effect of viscosity on external dispersion time constant, τ

Figure 4.1 Set-up for manual and automated blood sampling using a three-way stop cock.

Figure 4.2 Detail of set-up for manual and automated blood sampling. The short catheter on the distal end of the three-way stop cock is used for manual sampling.

Figure 4.3 Automated blood curve before (+) and after (o) decay correction.

Figure. 4.4 Illustration of importance of choosing calibration samples in the flat part of blood curve. A small timing error in the peak part (points A_1 and A_2) will yield a large difference in blood activity and lead to a large error in the calibration factor, F.

Figure 4.5 Procedure of calculating the calibration factor, F.

Figure 4.6 Comparison of a decay corrected and calibrated automated blood curve (•) with a manual one (+), also corrected for radioactivity decay.

Figure 4.7 An automated blood curve before (•) and after (o) dispersion correction (deconvolution).

Figure 4.8 Comparison of a smoothed (•) and unsmoohted (o) dispersion corrected (deconvolved) automated blood curve.

Figure 4.9 Comparison of a decay, delay and dispersion corrected smoothed automated blood curve (•) with the corresponding manual one (+). Note the excellent match of the two curves.

Figure 4.10 Comparison of FWHM for automated and manual blood curve from CMR_{O_2} study.

Figure 5.1 Manual blood curve with a timing error of +2 s (□) and -2 s (o) (• is the original curve).

Figure 5.2 Example of a CBF image of one brain slice from a young volunteer

generated from automated blood data.

Figure 5.3 Example of a CMR_{O_2} image of one brain slice from a young volunteer generated from automated blood data.

LIST OF TABLES

Table 4.4 Comparison of FWHM for automated and manual blood curves used to obtain CMR_{O_2} images.

Table 5.1 Percentage error in whole brain CBF values resulting from manual blood curves with a $\pm$ 2 s sample timing error.

Table 5.2 Whole brain CBF values ($ml \cdot hg^{-1} \cdot min^{-1}$) obtained from seven young volunteers using automated and manual blood data.

Table 5.3 Whole brain CMR_{O_2} values ($\mu mol \cdot hg^{-1} \cdot min^{-1}$) obtained from seven young volunteers using automated and manual blood data.

REFERENCES

1. Hoffman E.J., Phelps M.E.: Positron emission tomography: Principles and quantification. In: Phelps M.E., Mazziotta J.C., Schelbert H.R. (eds) Positron emission tomography studies in the brain: Positron Emission Tomography and Autoradiography: Principles and Applications for the Brain and Heart. Raven Press, New York, 237-286, 1986

2. Wrenn F.R. Jr., Good M.L., Handler P.: Use of positron-emitting radioisotopes for localization of brain tumors. *Science* 113:525-528, 1951

3. Sweet W.H., Brownell G.L.: Localization of intracranial lesion by scanning with positron-emitting arsenic. *J Am Med Assoc* 157:1183-1187, 1955

4. Yamamoto Y.L., Robertson J.S.: Study of quantitative assessment of section micro-regional cerebral blood flow in man by multiple positron detecting system using krypton-79. *BNL Med Dept Circ No 28, Brookhaven National Laboratory, Islip, NY* 1966

5. Ohta S., Meyer E., Thompson C.J., Gjedde A.: Oxygen consumption of the living human brain measured after a single inhalation of positron emitting oxygen. *J Cereb Blood Flow Metab* 12:179-192, 1992

6. Meyer E.: ^{15}O studies with PET. In: Diksic M., Reba R.C. (eds) Radiopharmaceuticals and brain pathology studied with PET and SPECT. CRC

Press, Boca Raton Ann Arbor Boston 165-198, 1990

7. Gjedde A., Kuwabara H.: Kinetic analysis of glucose tracer uptake and metabolism by brain in vivo. In: Diksic M., Reba R.C. (eds) Radiopharmaceuticals and brain pathology studied with PET and SPECT. CRC Press, Boca Raton Ann Arbor Boston 135-164, 1990

8. Alpert N.M., Senda M., Correia J.A.: Mapping of local cerebral pH with positron emission tomography. In: Diksic M., Reba R.C. (eds) Radiopharmaceuticals and brain pathology studied with PET and SPECT CRC Press, Boca Raton Ann Arbor Boston 267-278, 1990

9. Brooks D.J., Lammertsma A.A., Beaney R.P., Leenders K.L., Buckingham P.D., Marshall J., Jones T.: Measurement of rigional cerebral pH in human subjects using continous inhalation of $^{11}CO_2$ and positron emission tomography. *J Cereb Blood Flow Metab* 4:458-465, 1984

10. Bustany P., Henry J.F., de Rotrou J., Signoret P., Cabanis E., Zarifian E., Ziegler M., Derlon JM., Crouzel C., Soussaline F., Comar D.: Correlation between clinical state and positron emission tomography measurement of local brain protein synthesis in Alzheimer's dementia, Parkinson's disease, schizophrenia and gliomas. In: Greitz T., Ingvar DH., Widen L., et al. (eds) The metabolism of the human brain studied with positron emission

tomography. Raven Press, New York 241-249, 1985

11. Gjedde A.: Kinetic analysis of radioligand binding in brain in vivo. In: Diksic M., Reba R.C. (eds) Radiopharmaceuticals and brain pathology studied with PET and SPECT. CRC Press 337-355, 1990

12. Evans A.C., Marret S., Neelin P., Collins L., Worsely K., Dai W., Milot S., Meyer E., Bub D.: Anatomical Mapping of Fuctional Activation in Stereotactic Coordinate Space *Neuroimage* 1:43-53, 1992

13. Schwaiger M., Hicks R.: The clinical role of metabolic imaging of the heart be positron imaging tomography *J Nucl Med* 32:565-576, 1991

14. Coleman R.E., Hoffman J.M., Hanson W.M., Sostman H.D., Schold S.C.: Clinival application of PET for the evaluation of brain tumors. *J Nucl Med* 32:616-622, 1990

15. Engel J Jr., Henry DR., Risinger MW., et al.: Presurgical evaluation for partial epilepsy: Relative contributions of chronic depth-electrode recordings versus FDG-PET and scalp-sphenoidal ictal EEG. *J Neurol* 40:1670-1677, 1990

16. Frackowiak R.S.: The pathophysiology of human cerebral ischemia, a new perspective obtained with positron emission tomography. *Q J Med* 57:713-727, 1985

17. Frackowiak R.S., Wise R.J.: Positron tomography in ischemic cere-

brovascular disease. *Neuro Clin* 1:183-200, 1983

18. Powers W.J., Raichle M.E.: Positron emission tomography and its application to the study of cerebrovascular disease in man. *Stroke* 16:361-376, 1985

19. Guttman M., Leger G.: PET studies of movement disorders. In. Diksic M., Reba R.C. (eds) Radiopharmaceuticals and brain pathology studied with PET and SPECT. CRC Press, Boca Raton Ann Arbor Boston 409-426, 1990

20. Farde L., Hall H., Ehrin E., Sedvall G.: Quantitative analysis of D_2 dopamine receptor binding in the living human brain by PET. *Science* 231:258, 1986

21. Wong D., Wagner H.N. Jr., Tune L.E., Dannals R.F., Pearlson G.D., Links J.M., Tamminga C.A., Broussole E.P., Ravert H.T., Wilson A.A., Toung J.K.T., Malat J., Williams J.A., O'Tuama L., Synder S.H., Kuhar M.J., Gjedde A.: Positron emission tomography reveals elevated D_2 dopamine receptors in drug-naive schizophrenics. *Science* 234:1558, 1986

22. Weiss D.W., Souder E., Alavi A.: Regional cerebral metabolic and structural changes in normal aging and dementia as detected by PET and MRI In: Diksic M., Reba R.C. (eds) Radiopharmaceuticals and brain pathology stud-

ied with PET and SPECT. CRC Press, Boca Raton Ann Arbor Boston 409-426, 1990

23. Leblanc R., Meyer E., Bub D., Zatorre R., Evans A.C.: Language localization with activation positron emission tomography scanning. *Neurosurgery* 31:369-373, 1992

24. Leblanc R., Meyer E.: Functional PET scanning in the assesment of cerebral arteriovenous malformations. *J Neurosurg* 7:615-619, 1990

25. Herscovitch P., Markham J., Raichle M.E.: Brain blood flow measured with intravenous $H_2{}^{15}O$. I. Theory and error analysis. *J Nucl Med* 24:782-789, 1983

26. Raichle M.E., Martin W.R.W., Herscovitch P., Mintun M.A., Markham J.: Brain blood flow measured with intravenous $H_2{}^{15}O$. II. Implementation and validation. *J Nucl Med* 24:790-798, 1983

27. Jones T., Chesler D.A., Ter-Pogossian M.M.: The continuous inhalation of oxygen-15 for assessing regional oxygen extraction in the brain of man. *Br J Radiol* 40:339-343, 1976

28. Frackowiack R.S.L., Lenzi G.L., Jones T., Heather J.D.: Quantitative measurement of regional cerebral blood flow and oxygen metabolism in man using O-15 and positron emission tomography. Theory, procedure, and normal

values. *J Comput Assist Tomogr* 4:727-736, 1980

29. Koeppe R.A., Holden J.E., Polcyn R.E., Nickles R.J., Hutchins G.D., Weese J.L.: Quantitation of local cerebral blood flow and partition coefficient without arterial sampling: Theory and validation. *J Cereb Blood Flow Metab* 5:214-224, 1985

30. Iida H., Kanno I., Miura S., Murakami M., Takahashi K., Inugami A., Shishido F., Uemura K.: An accurate determination of regional brain/blood partition coefficient of water using dynamic positron emission tomography: validation of Kety-Schmidt single compartment model for $H_2{}^{15}O$ based on measurement. *J Cereb Blood Flow Metab* 7:S576, 1987

31. Lammertsma A.A., Frackowiak R.S.J., Hoffman J.M., Huang S.C., Weinberg I.N., Dahlbom M., MacDonald N.S., Hoffman E.J., Mazziotta J.C., Heather J.D., Forse G.R., Phelps M.E., Jones T.: The $C^{15}O_2$ build-up technique to measure regional cerebral blood flow and volume of distribution of water. *J Cereb Blood Flow Metab* 9:461-470, 1989

32. Hutchins G.D., Hichwa R.D., Koeppe R.A.,: A continuous flow input function detector for $H_2{}^{15}O$ blood flow studies in positron emission tomography *IEEE Trans Nucl Sci* 33:546-549, 1986

33. Kanno I., Iida H., Miura S., Murakami M., Takahashi K., Sasaki H., Inugami A., Shishido F., Uemura K.: A system for cerebral blood flow measurement using an $H_2{}^{15}O$ autoradiographic method and positron emission tomography. *J Cereb Blood Flow Metab* 7:143-153, 1987

34. Eriksson L., Holte S., Bohm C.H.R., Kesselberg M., Hovander B.: Automated blood sampling system for positron emission tomography. *IEEE Trans Nucl Sci* NS-38:703-707, 1988

35. Nelson A.D., Muzic R.F., Miraldi F., Muswick G.J., Leisure G.P., Voelker W.: Continuous arterial positron monitor for quantitation in PET imaging. *Am J Physio Ima* 5:84-88, 1990

36. Mazzictta J.C., Phelps M.E.: Positron emission tomography studies of the brain. In: Phelps M.E., Mazziotta J.C., Schelbert H.R. (eds) Positron emission tomography studies in the brain: Positron Emission Tomography and Autoradiography: Principles and Applications for the Brain and Heart.Raven Press, New York, 493-579, 1986

37. Kety S.S.:The theory and application of the exchange of inert gas at the lungs and tissue. *Pharmacol Rev* 3:1-41, 1951

38. Kety S.S.:Measurement of local blood flow by the exchange of an inert,

diffusible substance. *Meth Med Res* 3:228-236, 1960

39. Eichling J.O., Raichle M.E, Grubb R.L. Jr., Ter-Pogossian M.M.: Evidence of the limitations of water as a freely diffusible tracer in brain of the Rhesus monkey. *Circ Res* 35:358-364, 1974

40. Ohta S., Meyer E., Gjedde A.: Weighted integration method with CBV correction to estimate rCBF by PET. *Eur J Nucl Med* 16: iii s178, 1990

41. Alpert N.M., Eriksson L., Chang J.Y., Bergström M., Litton J.E., Correia J.A., Bohm C., Ackerman R.H., Tavers J.M.: Strategy for the measurement of regional cerebral blood flow using short-lived tracers and emission tomography. *J Cereb Blood Flow Metab* 4:28-34, 1984

42. Meyer E.: Simultaneous correction for tracer arrival delay and dispersion in CBF measurements by the $H_2{}^{15}O$ autoradiographic method and dynamic PET. *J Nucl Med* 30:1069-1078, 1989

43. Iida H., Higano S., Tomura N., Shishido F., Kanno I., Miura S., Murakami M., Takahashi K., Sasaki H., Uemura K.: Evaluation of regional differences of tracer appearance time in cerebral tissue using [^{15}O] water and dynamic positron emission tomography. *J Cereb Blood Flow Metab* 8:285-288, 1988

44. Iida H., Kanno I., Miura S., Murakami M., Takahashi K., Uemura

K.:Error analysis of a quantitative cerebral blood flow measurement using $H_2{}^{15}O$ autoradiography and positron emission tomography, with respect to the dispersion of the input function. *J Cereb Blood Flow Metab* 6:536-545, 1986

45. Ter-Pogossian M.M., Eichling J.O., Davis D.O., Welch M.J.: The measure in-vivo of regional cerebral oxygen utilization by means of oxyhemoglobin labeled with radio-active oxygen-15. *J Clin Invest* 49:381-391,1970

46. Raichle M.E., Grubb R.L.Jr., Eichling J.O., Ter-Pogossian M.M.: Measurement of brain oxygen utilization with radioactive oxygen-15: Experimental verification. *J Appl Physiol* 40:638-640, 1976

47. Mintun M.A., Raichle M.E., Martin W.R.W., Herscovitch P.: Brain oxygen utilization measured with O-15 radiotracers and positron emission tomography *J Nucl Med* 27:177-187, 1984

48. Huang S., Feng D., Phelps M.E.: Model dependency and estimation reliability in measurement of cerebral oxygen utilization rate with oxygen-15 and dynamic positron emission tomography. *J Cereb Blood Flow Metab* 6:105-119, 1986

49. Meyer E., Tyler J.L., Thompson C.J., Redies C., Diksic M., Hakim A.M.: Estimation of cerebral oxygen utilization rate by single-bolus $^{15}O_2$ inhalation and dynamic positron emission tomography. *J Cereb Blood Flow*

Metab 7:403-414, 1987

50. Kanno I., Miura S., Yamamoto S., Iida H., Murakami M., Takahashi K., Uemura K.: Design and evaluation of a positron emission tomograph: Headtome III. *J Comput Assist Tomogr* 9:931-939, 1985

51. Holte S., Eriksson L., Litton J.: An automated blood sampling system for positron emission tomography. *IEEE Trans Nucl Sci* 1988

52. Weast R.C., Astle M.J., Beyer W.H. (eds) CRC Handbook of chemistry and physics. CRC Press, 65^{th} edition, F35-F44, 1985

53. Fishman G.S.: Sampling from the poisson distribution of a computer *Computing* 17:147-156, 1976

54. Evans A.C., Thompson C.J., Marrett S., Meyer E., Mazza M.: Performance evaluation of the PC-2048: A new 15-slice encoded crystal PET scanner for neurological studies. *IEEE Trans Med Imaging* 10:89-98, 1991

55. Cooke B.E., Evans A.C., Fanthome E.A., Alarie R., Sendyk A.M.: Performance figures and images from the Therascan 3128 positron emission tomograph. *IEEE Trans Nucl Sci* NS-32:640-644, 1984

56. Sayers B.McA.: Inferring significance from biological signals. In. Clynes M. (ed) Biomedical engineering systems. McGraw-Hill, New York, 84 115, 1970

57. **Burton A.C.**: Physiology and biophysics of the circulation. Year Book Medical Publisher Chapter 5, Chicago, 1965

58. **Vafaee M., Meyer E., Gjedde A.**: O-15 water and O-15 labelled red blood cells require separate external dispersion corrections. Accepted for oral presentation at the SNM Annual Meeting, Toronto, June 1993.

APPENDIX I

AUTOMATED BLOOD FILE

a	b	c	d	e	f	g	h	i	j
35873.02	0 00	0.50	0	57	64	0	82	67	0
35873.52	0.50	0.50	0	39	56	0	87	73	0
35874.02	1.00	0.50	0	47	54	0	76	40	0
35874 52	1 50	0.50	0	37	61	0	79	55	0
35875.02	2.00	0.50	0	43	72	0	73	53	0
35875.52	2 50	0.50	0	44	58	0	86	54	0
35876.02	3.00	0.50	0	48	91	0	80	67	0
35876 52	3.50	0.50	0	61	65	0	82	79	0
35877.02	4.00	0.50	0	62	78	0	103	65	0
35877.52	4.50	0.50	0	68	80	0	93	86	0
35878.02	5.00	0.50	0	82	87	0	92	91	0
35878.52	5 50	0.50	0	84	73	0	102	73	0
35879.02	6.00	0.50	0	79	109	0	127	98	0
35879.52	6.50	0.50	0	88	108	0	123	95	0
35880.02	7.00	0.50	0	113	139	0	148	129	0
35880 52	7 50	0.50	0	141	178	0	175	144	0
35881.02	8.00	0.50	0	182	209	0	191	196	0
35881.52	8 50	0.50	1	190	228	2	237	196	0
35882.02	9.00	0.50	0	232	238	0	239	250	0
35882.52	9.50	0.50	0	218	244	2	276	248	0
35883.02	10.00	0.50	0	254	294	1	318	275	0
35883.52	10.50	0.50	0	253	309	5	293	243	0
35884.02	11 00	0.50	0	268	300	2	334	304	0
35884.52	11.50	0.50	0	268	322	2	330	275	0
35885.02	12.00	0.50	1	282	322	0	320	298	0
35885.52	12.50	0.50	1	306	351	0	376	338	0
35886.02	13.00	0.50	1	349	442	1	458	379	0
35886 52	13 50	0.50	0	369	435	9	458	383	0
35887.02	14.00	0.50	3	408	443	13	478	439	0
35887.52	14.50	0.50	4	438	515	1	481	426	0
35888.02	15.00	0.50	5	391	505	7	539	457	0
35888 52	15.50	0.50	1	434	538	5	498	450	0
35889.02	16.00	0.50	1	443	541	3	571	458	0
35889.52	16.50	0 50	1	434	527	6	549	481	0
35890.02	17.00	0.50	0	477	593	1	586	463	0
35890.52	17.50	0.50	4	438	513	2	567	492	0
35891.02	18.00	0.50	7	459	497	1	548	477	0
35891.52	18.50	0.50	6	453	584	8	598	478	0
35892.02	19.00	0.50	8	506	566	3	571	444	0
35892.52	19.50	0.50	7	457	574	5	602	529	0
35893.02	20.00	0.50	19	627	628	16	638	587	0
35893.52	20.50	0.50	28	633	725	28	706	582	0
35894.02	21.00	0.50	50	718	785	38	776	670	0
35894.52	21.50	0.50	75	766	921	63	883	803	0
35895.02	22.00	0.50	113	859	1011	91	948	918	0
35895.52	22 50	0.50	147	1020	1144	127	1079	1045	0
35896.02	23.00	0.50	196	1244	1373	142	1219	1124	0
35896.52	23.50	0.50	242	1398	1584	213	1433	1414	0
35897.02	24.00	0.50	335	1762	1917	248	1694	1639	0
35897.52	24.50	0.50	365	2028	2188	333	1992	1877	0
35898.02	25.00	0.50	480	2336	2470	423	2305	2242	0

a. Time of the day in seconds
b. Time since start in seconds
c. Sampling interval in seconds
d. Coincidence count in the first detector pair
e. Singles count in the first detector pair, first detector
f. Singles count in the first detector pair, second detector
g. Coincidence count in the second detector pair
h. Singles count in the second detector pair, first detector
i. Singles count in the second detector pair, second detector
j. Acquired count from the auxillary input

APPENDIX II

PROGRAMS "**RANO.FOR**" FOR RANDOM NUMBER GENERATION AND "**GASDEV.FOR**" FOR NORMAL DISTRIBUTION

```
C-------------------------------------------------------------------
C----------------------------RANO.FOR-------------------------------
C    Returns a uniform random deviate between 0.0 and 1.0 using a
C         system-supplied routine RAN(ISEED). Set IDUM to any
C              negetive value to initialize the sequence.
C-------------------------------------------------------------------
C-------------------------------------------------------------------

      function rano(idum)

      dimension v(97)
      data iff /0/
C-------------------------------------------------------------------
               if(idum.LT.0.or.iff.eq.0) then
      iff = 1
      iseed = abs(idum)
      idum = 1
      do 11 j = 1,97
               dum = ran(iseed)
11    continue
      do 12 j = 1,97
      v(j) = ran(iseed)
12    continue
      y = ran(iseed)
               end if
C-------------------------------------------------------------------
      j = 1 + int(97.*y)
      if(j.GT.97.or.j.LT.1)pause
      y = v(j)
      rano = y
      v(j) = ran(iseed)
      return
      end
```

```
C-----------------------------------------------------------------
C-----------------------GASDEV.FOR--------------------------------
C  Returns a normally distributed deviate with zero mean and unit
C     variance, using RANO as the source of uniform diviates.
C-----------------------------------------------------------------
C-----------------------------------------------------------------
      real function gasdev(idum)
C-----------------------------------------------------------------
      implicit none

      integer*4  iset,idum

      real*4 v1,v2,rano,r,fac,gset
C-----------------------------------------------------------------
      data iset/0/
          if (iset.EQ.0) then
1             v1 = 2.*rano(idum) - 1.
              v2 = 2.*rano(idum) - 1.
              r = v1**2 + v2**2
          if(r.GE.1..or.r.EQ.0.) go to 1
              fac = sqrt(-2.*log(r)/r)
              gset = v1*fac
              gasdev = v2*fac
              iset = 1
      else
              gasdev = gset
              iset = 0
      end if
C-----------------------------------------------------------------
      return
      end
```

APPENDIX III

PROGRAM "**MAINFITGAS.FOR**" FOR DETERMINATION OF SIMULATED DISPERSION TIME CONSTANT USING STEP RESPONSE OF ACTIVITY

```
C-----------------------------------------------------------------
C----------------------MAINFITGAS.FOR-----------------------------
C        PROGRAM TO FIT STEP RESPONE OF ACTIVITY IN ORDER
C              TO DETERMINE DISPERSION TIME CONSTANT
C-----------------------------------------------------------------
C-----------------------------------------------------------------
      DIMENSION Y(200),X(200),A(50),DELTAA(50),SIGMAA(50),YFIT(20
     1 SIGMAY(200),TI(200),CO(200)
      character*120 input_file,fitted_file

120     format(120a)
106     format(1x,3f10.4)
550     format(3x,'ENTER INPUT FILE NAME:..... ',$)
600     format(3x,'ENTER FITTED FILE NAME:..... ',$)
605     format(3x,'ENTER CONSTANTS.....: ',$)
606     format(3x,'ENTER MODE....: ',$)
C607    format(3x,'ENTER MODE....: ',$)
608     format(3x,'ENTER NPTS....: ',$)
609     format(3x,'ENTER NTERMS....: ',$)

C-----------------------------------------------------------------
              write(6,550)
              read(5,120)input_file
          open(unit=1, name=input_file, type='old', readonly)
                write(6,600)
              read(5,120)fitted_file
          open(unit=9, name=fitted_file, type='new')
C               write(6,605)
C             read(5,*)npts,nterms,mode,sigmaa,sigmay
                write(6,606)
                read(5,*)mode
C               write(6,607)
C               read(5,*)
                write(6,608)
                read(5,*)NPTS
                write(6,609)
                read(5,*)NTERMS
C       do 11 i=1,npts
C-----------------------------------------------------------------
C         read(1,*)X(I),Y(I)
C         y(I)=y(I)+((0.1*Y(I))*(RANO(I)-0.5))
C         type *,X(i),Y(i)
C=================================================================
C         NPTS=100
C         NTERMS=2
C    13   MODE=0
      TYPE *,'NPTS:','NTERMS:','MODE:',NPTS,NTERMS,MODE
      DO 100 I=1,NTERMS
      TYPE *,'TEST'
      A(I)=1.0
      SIGMAA(I)=1.0
```

```
      DELTAA(I)=0.1
  100 CONTINUE
C     WRITE(6,15)
C 15  FORMAT(3X,'A')
      WRITE(6,16) A(1),A(2)
   16 FORMAT(F10.3,5X,F10.3)
   20 DO 50 I=1,NPTS
      X(I)=I-1
      Y(I)=A(1)*(1.0-EXP(-X(I)*A(2)))
C      dumi=555
      y(I)=y(I)+((0.05*Y(I))*(gasdev(dumi)-0.5))
      SIGMAY(I)=1.0
   50 CONTINUE
C     type *,'DUMI:',dumi
      DO 110 I=1,NTERMS
      TYPE *,'TEST1'
      A(I)=2.0
  110 CONTINUE
   3  DO 5 I=1,NPTS
      WRITE(6,36) X(I),Y(I)
   5  CONTINUE
   36 FORMAT(F10.4,5X,F10.4)
   200 CALL GRIDLS(X,Y,SIGMAY,NPTS,NTERMS,MODE,A,DELTAA,SIGMAA,YFI
     1 CHISQR)
C     TYPE PARAMETERS
      TYPE *,'CHISQR:',CHISQR
      WRITE(6,250)
  250 FORMAT(3X,'TIME',9X,'ACTIVITY',9X,'YFIT')
  300 DO 502 I=1,NPTS
      WRITE(6,350) X(I),Y(I),YFIT(I)
      write(9,350) X(I),Y(I),YFIT(I)
  502 CONTINUE
  350 FORMAT(F10.4,5X,F10.4,5X,F10.4)
      WRITE(6,551) A(1),A(2)
  551 FORMAT(F10.4,3X,F10.4)
      close(1)
      close(9)
      STOP
     END
```

APPENDIX IV

PROGRAM "**GET_CALBLD.FOR**" FOR CALIBRATION OF BLOOD CURVE ALONG WITH THE CALIBRATION SHEET

```
c-------------------------------------------------------------
c---------------------GET_CALBLD.FOR--------------------------
c        PROGRAM FOR CALIBRATION OF THE DECAY CORRECTED
c                        BLOOD FILE
c-------------------------------------------------------------
c-------------------------------------------------------------
        character*120 cnt

120     format(120a)
106     format(2f10.1)
601     format(3x,'Enter DECAY CORRECTED BLD file name ..... :
603     format(3x,'Enter CALIBRATED BLD file name ..... : ',$)
605     format(3x,'Enter Constants..... : ',$)

        real B,d
c-------------------------------------------------------------
            write(6,601)
            read(5,120)cnt
        open(unit=1, name=cnt, type='old', readonly)
            write(6,603)
            read(5,120)cnt
        open(unit=3, name=cnt, type='new')
            write(6,605)
            read(5,*)a1,a2,a3,a4,b1,b2,b3,b4

        do 11 i = 1,500
c-------------------------------------------------------------
            read(1,*,end=119)ti,act
c "ti" and "act" are time and activity from the decay corrected
c  blood file

         f =(a1*b1+a2*b2+a3*b3+a4*b4)/(a1*a1+a2*a2+a3*a3+a4*a4)
         b = act*f
11                  write(3,106)ti,b

c-------------------------------------------------------------
119     close(1)
        close(3)
        type *,'calibration factor = ',f
        stop
        end
c-------------------------------------------------------------
```

DATE:

STUDY:

SUBJECT:

CALIBRATION DATA

No.	START	STOP
1		
2		
3		
4		
5		

APPENDIX V

PROGRAM "GET_DELCONSMO.FOR" AND RELATED SUBROUTINES FOR EXTERNAL DELAY AND DISPERSION CORRECTION

```
C-------------------------------------------------------------
C----------------------GET_DELCONSMO.FOR----------------------
C          READS CALIBRATED BLOOD CURVE AND APPLIES DELAY
C            AND DECONVOLUTION PROCESS ON IT PRODUCING A
C               SMOOTHED VERSION PLUS ITS DERIVATIVE
C-------------------------------------------------------------
C-------------------------------------------------------------
C           SET NEGATIVE VALUES OF CTRU TO ZERO
C           OTHER MODULES REQUIRED:DREDBLD,DERIV
C      X,Y  : ORIGINAL NON-UNIFORM TIME SEQUENCE
C      XU,YU: UNIFORMLY INTERPOLATED DATA SEQUENCE
C      YFIT : SMOOTHED UNIFORM DATA SEQUENCE AT TIMES XU
C      Z    : SMOOTHED UNIFORM DERIVATIVE AT TIMES XU
C      CTRU : TRUE, DECONVOLVED INPUT FUNCTION AT TIMES XU


      DIMENSION X(400),Y(400),YFIT(400),Z(400),CTRU(400),CAL(3)
C     DIMENSION XU(400),YU(400),CAL(3)
      LOGICAL*1 FILNAM(32),TEXT(72)


C     READ BLOOD DATA Y(I) AT TIMES T(I).
      TYPE 10
10    FORMAT(/'$   ENTER DECAY CORRECTED AND CALIBRATED BLOOD FIL

         CALL DREDBLD(X,Y,CAL,NPTS)
      DO 15 I=1,NPTS
      WRITE(6,16) X(I),Y(I)
15      CONTINUE

16    FORMAT(F10.1,5X,F10.1)
C     SET NUMBER OF POINTS TO FIT OVER:NN=3 (NO SMOOTHING).
C     NN=3
      TYPE 17
17    FORMAT(/'$   ENTER NUMBER OF POINTS TO FIT (UNEVEN):')
      ACCEPT *,NN
C     SET EQUIDISTANT TIME INTERVAL FOR BLOOD CURVE TO DT=0.5 SEC
      DT=0.5
C     TYPE 19

19    FORMAT(/'$   ENTER DISPERSION CONSTANT TAU (SEC)    :')
C     ACCEPT *,TAU
C     SET DISPERSION CONSTANT TAU TO 5.5 SEC.
C     SEQUENCE XU(I), YU(I) WITH DT=0.5 SEC.


C     FORM SMOOTHED VERSION PLUS DERIVATIVE.

            CALL DERIV2(NN,NPTS,Y,YFIT,Z,DT)
C     PRINT SMOOTHED DATA PLUS DERIVATIVE.
C     FORM CTRU(I)=YFIT(I)+TAU*Z(I)
           DO 100 I=1,NPTS
100   TYPE 1,X(I),Y(I)
           DO 200 I=1,NPTS-NN/2
```

```
      CTRU(I)=YFIT(I)+TAU*Z(I)
           IF (CTRU(I) .LT. 0.) CTRU(I)=0.
200   TYPE 2,X(I),Y(I),YFIT(I),Z(I),CTRU(I)


1     FORMAT(2F10.1)
2     FORMAT(5F10.1)
C     WRITE CTRU(I) INTO NEW BLOOD DATA FILE WITH NEW NAME.
           TYPE 111
111   FORMAT(/'$   ENTER NEW DECONVOLVED BLOOD FILE NAME:')
           READ(5,22)IQ,FILNAM
22    FORMAT(Q,32A1)
      LUN=1
      FILNAM(IQ+1)=0
      OPEN(UNIT=LUN1,NAME=FILNAM,TYPE='NEW',FORM='FORMATTED')
      NTEXT=4
      WRITE(LUN1,9)NTEXT
9     FORMAT(I7)
      WRITE(LUN1,8)
8     FORMAT(/' DECONVOLVED BLOOD ACTIVITY DATA (CPS/G) '//)
      WRITE(LUN1,11)(CAL(I),I=1,3)
11    FORMAT(3F)
C     WRITE BLOOD DATA INTO OUTPUTFILE.
          DO 1000 I=1,NPTS-NN/2


C     APPLY DELAY CORRECTION
          X(I)=X(I)-4.5
1000  WRITE(LUN1,105)X(I),CTRU(I)
105   FORMAT(2F10.1)
      CLOSE(UNIT=LUN1,DISPOSE='KEEP')
      STOP
      END
```

```
C-------------------------------------------------------------
C               SUBROUTINE DERIV2.FOR
C-------------------------------------------------------------
C      PERFORMS SMOOTHING AND CALCULATES DERIVATIVE OF A CURVE
C      USING PARABOLIC REGRESSIVE FILTER APPROACH.(SEE: SAYERS,
C      INFERRING SIGNIFICANCE FROM BIOLOGICAL SIGNAL(FILTERS).
C-------------------------------------------------------------


      SUBROUTINE DERIV2(NN,NPTS,Y,YFIT,Z,DT)

      DIMENSION Y(400),YFIT(400),Z(400)
      ANN=FLOAT(NN)
      CAA=3./(4.*ANN*(ANN*ANN-4.0))
      CBB=12./(ANN*(ANN*ANN-1.0))
      JBEG=(NN+1)/2
      JEND=NPTS-JBEG+1
          DO 265 I=1,NPTS
      YFIT(I)=0.
      Z(I)=0.
265   CONTINUE
          DO 300 I=JBEG,JEND
      AA=0.
      BB=0.
      CC=0.
          DO 280 J=1,NN
      JJ=J-1
      KK=-((NN-1)/2)+JJ
      AKK=FLOAT(KK)
      AA=AA+Y(I+KK)*(3.*ANN*ANN-20.*AKK*AKK-7.)
      BB=BB+Y(I+KK)*AKK
280   CONTINUE
      YFIT(I)=CAA*AA
      Z(I)=CBB*BB/DT
300   CONTINUE
      RETURN
      END
```

```
C-------------------------------------------------------------
C              SUBROUTINE DREDBLD.FOR
C-------------------------------------------------------------

     SUBROUTINE DREDBLD(X,Y,CAL,NPT)
     LOGICAL*1 FILNAM(32),TEXT(72)
     REAL*4 CAL(3),X(400),Y(400)
C
     READ(5,2)IQ,FILNAM
2    FORMAT(Q,32A1)
C
     LUN=1
     FILNAM(IQ+1)=0
     OPEN(UNIT=LUN,NAME=FILNAM,TYPE='OLD',READONLY)
     READ(LUN,20)NTEXT
20   FORMAT(I)
        DO 22 I=1,NTEXT
     READ(LUN,21)TEXT
21   FORMAT(72A1)
22   CONTINUE
C
     READ(LUN,35)(CAL(I),I=1,3)
35   FORMAT(3F)
     TYPE *,' Calibration factors are ',CAL(1),CAL(2),CAL(3)

C37  TYPE 36
C36  FORMAT(/'$ Lower,Central or Upper data?( type 1,2 or 3).. '
C    ACCEPT *,IC
C    IF(IC.LT.1.OR.IC.GT.3)GOTO 37
C    SC=CAL(IC)
     IPT=0
5    IPT=IPT+1
     READ(LUN,10,END=200)XX,YY
     X(IPT)=XX
C    Y(IPT)=YY*SC
     Y(IPT)=YY
10   FORMAT(2F10.4)
C    TYPE *,XX,YY
     GOTO 5
200  NPT=IPT-1
     CLOSE(UNIT=LUN,DISPOSE='KEEP')
     RETURN
     END
```